Title

Analysis of hippocampal place cell dysfunction in mouse models of Alzheimer’s disease through single unit electrophysiology and calcium imaging techniques

Author

Gaur, Kshitij Sudhakar

Publication Date

2019

Peer reviewed|Thesis/dissertation

UNIVERSITY OF CALIFORNIA SAN DIEGO

Analysis of hippocampal place cell dysfunction in mouse models of Alzheimer's disease through single unit electrophysiology and calcium imaging techniques

A Thesis submitted in partial satisfaction of the requirements
for the degree Master of Science

in

Biology

by

Kshitij Gaur

Committee in charge:

Professor Stefan Leutgeb, Chair
Professor Jill Leutgeb
Professor Cory Root

2019

The Thesis of Kshitij Gaur is approved, and it is acceptable in quality and form for publication on microfilm and electronically:

Chair

University of California San Diego

2019

DEDICATION

To my parents

Without you, I would be nowhere. For your constant advice, guidance, and support, I would like to dedicate my dissertation to you. Thank you for everything you have given me.

TABLE OF CONTENTS

LIST OF ABBREVIATIONS

HPC	Hippocampus
APP	Amyloid Precursor Protein
AD	Alzheimer's Disease
SWR	Sharp Wave Ripple
IACUC	Institutional Animal Care and Use Committee
GECI	Genetically Encoded Calcium Indicator
AB-42	Amyloid Beta-42
AB-40	Amyloid Beta-40
NFT	NeuroFibrillary Tangle
PSEN	Presinilin
LTP	Long Term Potentiation
GRIN	Gradient Index
AP	Anteroposterior
ML	Mediolateral
DV	Dorsoventral
LFP	Local field potential
DG	Dente Gyrus
PFA	4% Paraformaldehyde
PBS	Phosphate Buffered Saline
AAV	Adeno-Associated Virus

LIST OF FIGURES

ACKNOWLEDGEMENTS

I would like to acknowledge Professor Stefan Leutgeb for serving as the chair of my committee and acting as the principal investigator for my project. Thank you for your constant support and advice as I embarked on a journey to become a more independent researcher. After four years in your lab, I can confidently say that being in your lab has been one of the most rewarding experiences I could have ever had in my young educational career.

I would also like to acknowledge Professor Jill Leutgeb and Professor Cory Root for being a part of my committee as well. Your support is a reminder of the impact that collaboration has on advancing science.

Finally, I would like to acknowledge Dr. Silvia Viana da Silva. I am so honored to have had you as my mentor during my time in the Leutgeb laboratory. You were patient with me when I struggled, enthusiastic when I succeeded, and you were always present to guide me through every step of my journey. I could not have asked for a more inspiring role model. I owe everything I have ever achieved in this lab to you. Without you, none of this would have been possible.

This thesis, in full, is currently being prepared for submission of publication of the material by Viana da Silva, Silvia; Haberl, Matthias G; Gaur, Kshitij S; Patel, Rina; Koo, Edward; Leutgeb, Jill K.; Leutgeb, Stefan. The author of this thesis will be a co-author of the publication.

VITA

2015-2016	Instructional Apprentice, Department of Biological Sciences, University of California San Diego
2016-2018	Tutor, Department of Biological Sciences, University of California San Diego
2018	Bachelor of Science, University of California San Diego
2018-2019	Teaching Assistant, Department of Biological Sciences, University of California San Diego
2019	Master of Science, University of California San Diego

FIELD OF STUDY

Major Field: Biology

Studies in Neurobiology and Neurophysiology
Professors Jill Leutgeb and Stefan Leutgeb

ABSTRACT OF THE THESIS

Analysis of hippocampal place cell dysfunction in mouse models of Alzheimer's disease through single unit electrophysiology and calcium imaging techniques

by

Kshitij Gaur

Master of Science in Biology

University of California San Diego, 2019

Professor Stefan Leutgeb, Chair

Alzheimer's disease (AD) is a neurodegenerative disease characterized by progressive mnemonic deficits. Previous studies have established that AD causes neural dysfunction in hippocampal place cells in the form of decreased place cell stability and increased place field size in mouse models. Most such experiments, however, have been unable to record from specific layers of the hippocampus while AD mouse models complete goal-oriented spatial memory tasks. Here, we introduced a spatial memory task to allow electrophysiology recordings from the CA1, CA3, and DG regions of the hippocampus while transgenic mouse models expressing AD-pathology in hippocampal CA3 (CA3-APP animals) completed the task. We also aimed to apply calcium imaging to

analyze populations of place cells from the CA1 region in order to compare calcium imaging data to tetrode wire electrophysiology data. We found that CA1 and CA3 place cells in CA3-APP animals showed impairments in firing rate, information score, stability, spatial discrimination, and place field size while animals completed hippocampal dependent memory tasks, particularly in aged animals. While our calcium imaging experiments were ultimately unsuccessful, we set the foundation for future calcium imaging experiments in this research. Our results thus suggest that substantial CA1 and CA3 place cell dysfunction occurs while CA3-APP animals complete hippocampal dependent spatial memory tasks. Furthermore, our experiments set the stage for using calcium imaging as method that can add to previously existing information about place cell dysfunction in AD and therefore paints a more global image of hippocampal dysfunction in AD.

INTRODUCTION

Alzheimer's disease (AD) is a neurodegenerative disorder that is characterized by progressive mnemonic deficits. AD is the most common form of dementia in America (14 million diagnosed patients in 2014) and is projected to receive billions of dollars in funding every year for further study (Matthews et al., 2018). Part of the reason AD causes so much anxiety and grief among those afflicted can be explained by the scientific community's general lack of understanding surrounding the disease. Indeed, the cause and progression of AD is not clearly defined. This lack of understanding about the causes subsequently makes it difficult for researchers to diagnose early signs of AD and develop therapeutic treatments for patients suffering from the disease. Beginning in the hippocampal network (which is composed of both the hippocampus and the medial entorhinal cortex) and eventually spreading to all cortices of the brain, AD is thought to be characterized by a buildup of extracellular amyloid beta peptide (typically oligomers of 40-42 peptides in length), which is then associated with a resulting build-up of intracellular tau neurofibrillary tangles (NFTs). This resulting buildup is thought to lead to many of the symptoms commonly associated with AD, though the link between amyloid beta peptide and NFTs and neurodegenerative symptoms is not entirely clear. There is some evidence that suggests that the buildup of amyloid beta peptide and NFTs leads to synaptic dysregulation and neuronal death, though further research is required to corroborate those claims. The prevailing hypothesis that buildup of Amyloid Beta peptide progresses to the neurodegenerative effects of AD in this fashion is collectively referred to as the amyloid cascade hypothesis (Hardy & Higgins, 1992).

The race to understand more about the neurogenesis and pathology of AD has led to numerous studies aiming to understand the mechanistic link between the presence of amyloid beta peptide and the ensuing neurodegenerative symptoms. Despite this, the ethical concerns of using humans already affected by AD poses a clear limitation in their use for experimentation. Furthermore, most AD diagnoses are made retrospectively (in other words, once the patient has already manifested several serious symptoms of the disease) (Götz & Ittner, 2008). This is problematic because it then becomes difficult to study the progression of the disease if patients have already shown serious neurodegenerative impairments. To combat this issue, researchers have turned towards mouse models that show similar phenotypic profiles as human AD patients. Two different forms of AD are currently characterized - sporadic and familial forms. Most mouse models of AD are based upon the familial form of AD, since it has well documented genetic mutations that drive its onset. Some of these mouse models were genetically engineered by causing them to express mutations in Presinilin-1 (PSEN-1) or Presinlin-2 (PSEN-2) - mutations commonly found on a ɣ-secretase enzyme in patients with familial onset AD (Götz & Ittner, 2008). These mutations can lead to improper cleavage of Amyloid Precursor Protein (APP) by corrupting ɣ-secretase activity, which is an enzyme involved in APP cleavage events. Another such enzyme is B-secretase, which is also responsible for cleaving APP. Generally, shifting activity to induce strain on B or ɣ-secretase is thought to increase production of AB-40/42 (Selkoe, 1991). A third secretase, α-secretase, is often involved in APP cleavage that is thought to be beneficial for neuronal health (Mattson et al., 1993; Furukawa et al., 1996). When properly cleaved, APP is known to play a key role in intracellular signaling events, as well as maintaining

homeostatic balance in the brain (Mattson et al., 1993; Furukawa et al., 1996; De Strooper & Annaert, 2000). However, the improper cleavage of APP into amyloid beta peptide of either 40 or 42 oligomers long is theorized to be at the heart of the amyloid cascade hypothesis. This is because oligomers of amyloid beta peptide at 40 or 42 peptides long have an increased propensity to aggregate into amyloid beta plaques (Roher et al., 1993). Improper cleavage of APP through mutations in PSEN are therefore used to cause an increase in production of AB-42 oligomers, which then aggregate into full AB plaques in order to model familial forms of AD. Despite the robust nature of this genetic manipulation in generating Alzheimer's-like pathology, researchers found that simply expressing PSEN mutations was not enough to develop the same extent of AB-40/42 production and plaque-like deposition as in human AD patients (De Strooper et al., 1995). Therefore, the field has developed mice that combined PSEN mutations as well as mutations in the APP gene found in patients with familial forms of AD. Researchers found that combining the Swedish mutation (K670N/M671L) (Mullan et al., 1992) with the Indiana mutation (V717F) on APP (Murrell et al., 1991) led to robust expression of Alzheimer's like pathology, with AB plaque deposition and cognitive deficits (Citron et al., 1992 & 1994; Cai et al., 1993; Johnston et al., 1994; Scheuner et al., 1996; Ancolio et al., 1999; Nilsberth et al., 2001). While other methods of modeling AD in mice exist (such as by increasing expression of an Apolipoprotein E isoform that is linked with increased risk of AD (ApoE4)), mutations in APP and PSEN remain the most pervasive methods used to generate AD pathology. For the work done in this thesis, mouse models expressing the Swedish and Indiana mutations on APP in the CA3 region of the hippocampus (CA3-APP animals) were used. Previous experiments in our laboratory

showed that CA3-APP animals showed robust expression of APP in the target hippocampal region and showed long term potentiation (LTP) impairments that increased with age. We decided to test the effects of APP overexpression in hippocampal CA3 because it directly manipulates synaptic plasticity in the CA1 region, thereby allowing us to test the effects of overexpressed mutant APP on the final computations of the trisynaptic pathway (the pathway through which neural information travels from the entorhinal cortex through the dentate gyrus, and CA3 and CA1 regions of the hippocampus), which is generally thought to be critical for supporting episodic memory (Ramon y Cajal, 1911). This is therefore a study of how loss of synaptic plasticity in the Schaeffer-Collateral synapse leads to AD-related impairments, rather than being an AD model in which all cells overexpress APP.

One use for animals models in studying the progression of AD pathology involves the use of tetrode wire microdrive recordings to record local field potential data in the hippocampal network of mice, where the inclusion of implantable tetrodes on the microdrive allows for separation of electrical signals to deduce neuronal activity from single units (single cells). The importance of the hippocampal network in memory and dementia research has long been established since the removal of the hippocampal network in the patient Henry Molaison (H.M.). After suffering from strokes due to a bicycle accident, surgeons removed the hippocampal network from H.M., and found that H.M. had immediate anterograde amnesia (the inability to encode new memories), while H.M. was still able to remember past events from before the surgery (Scoville & Milner, 1957). This implied that the hippocampal network was crucial for the processing of memory and pointed towards a hypothesis that the hippocampus was necessary for the

conversion of short-term memories into long term memories. With the importance of the hippocampus in memory research confirmed, decades of further research have begun unveiling the role of the hippocampus in dementia and memory disorders. With particular respect to these experiments, the hippocampal network was selected for study since it is one of the first known brain structures to be affected by progression of AD, and is central to mnemonic memory processing and spatial memory navigation (Scoville & Milner, 1957; O'Keefe et al., 1976; McNaughton & Morris, 1987; Eichenbaum, 2004; Leutgeb et al., 2005; Mu & Gage, 2011). A major breakthrough in the study of hippocampal physiology came in 1987 with the discovery of grid and place cells in the medial entorhinal cortex and hippocampus, respectively (O'Keefe et al., 1971, 1976 & 1978; Fyhn et al., 2004). Grid and place cells are particularly interesting neurons that code for specific environments, thus establishing a unique activation profile for every new setting their host organism finds themselves in (O'Keefe et al., 1978). This information is then conserved through long term potentiation (LTP) and synaptic enhancement events. Furthermore, it seems that previously encoded place cell ensembles potentiate themselves during periods of highly synchronous fast firing, causing what are known as sharp wave ripple events (SWRs) during non-rapid eye movement (NREM) sleep (Pavlides & Winson, 1989; Skaggs & McNaughton, 1996; Nádasdy et al., 1999; Buzsaki, G., 2006). Several previous studies have demonstrated that AD patients show significant deficits in spatial memory and navigation, which rely heavily upon place cell activity - thus implying that there may be a correlation between AD progression and place cell dysfunction (Liu et al., 1991; Grossi et al, 1993; Guariglia, 2007). This makes the study of place cells in the hippocampus a relevant target for research in AD.

Based on preliminary research using mouse models of AD, it is believed that inhibition of LTP and SWRs in hippocampal place cells may play a role in memory loss progression in AD mouse models (Chapman et al., 1999; Witton et al., 2015; Ciupek et al., 2015). Moreover, use of these models of AD induced significant grid cell dysfunction and neuron loss in the entorhinal cortex (part of the hippocampal formation), that are reminiscent of early stages of AD (Fu et al., 2017). These studies therefore suggested that place cell firing in the hippocampus is impaired in AD. To build upon this idea, several research teams established that AD mouse models show impaired hippocampal place cell physiology in the form of disturbed place cell firing patterns, stability, information score, and place field size (Cacucci et al., 2008; Ciupek et al., 2015). In those studies, however, electrophysiology data was collected while animals completed a forced alternation T-maze or Morris water maze, neither of which allow for electrophysiology data collection without interference from the experimenter during the task – a clear limitation of the studies. Other studies collected electrophysiology data during random foraging tasks that did not involve working memory. In other words, though the animals were required to process spatial information, these experiments did not directly test spatial memory. Furthermore, such experiments did not make a distinction between place cell deficits in CA1 or CA3 regions of the hippocampus. These experiments were then built upon by researchers suggesting that AD models showed impaired coordination and precision in CA1 pyramidal place cells while roaming freely through a circular maze and finding sugar (where the place cells coded place fields where the sugar pellets were located) (Mably et al., 2016). While this task involved spatial coding, it remains yet to be seen how hippocampal dysfunction progresses while completing goal-oriented working

memory tasks. It is further worth noting, that some experiments in rat models of AD showed that place cell dysfunction was more heavily implicated in the CA2/CA3 regions of the hippocampus, rather than in the CA1 region during a recognition memory task (Galloway et al., 2018). More exploration on which region of the hippocampus is most heavily implicated in place cell firing discrepancies is necessary to fully understand the extent to which all hippocampal regions are affected by AD. Furthermore, it will be important to understand how hippocampal place cell dysfunction occurs while animals complete goal-oriented working memory tasks, since it would elucidate aspects of memory loss progression in AD that have not yet been uncovered by most existing studies that use the aforementioned random foraging, water maze, or T-maze experiments. This is largely because, even though random foraging can still yield information about place coding, we hypothesize that it may be possible that there are different place cell computations for goal-oriented tasks. Since the aforementioned goal-oriented memory tasks do not allow for electrophysiology recordings while the animal is actually performing the task, electrophysiology data collected from those tasks would leave out analyses of place cell activity as place cell computations are being performed to complete the task. For the work done in this thesis, we therefore aimed to introduce a goal-oriented spatial memory task in the form of a continuous T-maze (figure 8 maze) that would allow us to analyze the computations CA1 and CA3 place cells may have to perform in order to receive a reward. We then hoped to analyze the deficits in place cell coding using the following spatial information metrics (metrics evaluating if firing of place cells can predict the location of an animal): information score, place field size, trial by trial stability, and spatial correlation in AD models.

Most of the preliminary data for AD model electrophysiology (and for other learning and memory studies) has been gathered using single unit electrophysiology recordings using the aforementioned tetrode wire microdrive implants. However, the number of cells that can be separated out and analyzed using tetrode wire electrophysiology is limited by the lack of proximal cells to the tetrode wires. An additional drawback of tetrode wire electrophysiology is that tetrode wires necessarily kill cells where they are implanted, preventing recording from those cells and derailing the possibility of recording those cells more than once after passing through the cell layer.

The apparent need to address these issues led to the development of Calcium imaging techniques in order to visualize neural ensembles in vivo. The calcium imaging technique is complemented by the development of a miniature microscope system (termed miniscope) that is implanted into the target brain region of the animal. When injected with a genetically induced Calcium indicator (GECI), transient increases in intracellular levels of Calcium during synaptic communication between neurons can be visualized using the miniscope, allowing for detection of all neurons that fire in response to a stimulus (Chen et al., 2013). Here, the increased intracellular calcium during action potential propagation binds to a calmodulin binding site of the GECI, which in turn undergoes a conformational change to express a genetically engineered GFP fluorophore (Miyawaki et al., 1997; Chen et al., 2013). This fluorescence can then be visualized during memory tasks using the miniscope (Ghosh et al., 2011). This is useful because it allows for the ability to visualize a large area of cells that have been injected with the GECI, and therefore gives a wider area from which researchers can see results.

Furthermore, this would allow researchers to visualize the cells in vivo during behavior tasks and examine sequences of place cell firing. Because of the transient expression of the GECI, and the lack of damage to surrounding tissue, the cells in the region should durably continue to fire over long periods of time, which could also allow for long term analysis of learning and memory. Not only that, this technique would allow for researchers to tag individual neuron subtypes and analyze those more specifically (eg. tagging interneurons or Cre-expressing neurons) (Tsien et al., 1996; Russel, J.T., 2011; Chen et al., 2013).

In the work done for this thesis, the GCaMP7f GECI was injected into the animals, since it was shown to have the fastest kinetics relative to other GECIs, therefore resulting in the highest possible temporal resolution. Furthermore, the miniscope is implanted in conjunction with a gradient index lens (GRIN lens), that allows for imaging of a flat neuronal surface area at multiple angles without distorting the optics (Cai et al., 2016). This method therefore allows for the simultaneous visualization and recording of a large population of single neurons over a significant period of time without degradation in signal strength. The usage of the GRIN lens in conjunction with a miniscope has already been utilized in several studies in sleep and memory research and has been established as a stable tool to record neural ensembles *in vivo* (Xu et al., 2016, Weber & Dan, 2016).

The goal of this study was therefore to first expand upon previously existing tetrode wire electrophysiology data by learning more about spatial information and place cell firing precision CA3-APP mouse models. We aimed to understand which place cell firing discrepancies occur during a spatial memory task to evaluate place cell function

while the cells are active during behavior. We also hoped to elucidate which structures of the hippocampus saw the most striking place cell firing dysfunction. We then hoped to compare the information received using tetrode wire electrophysiology with miniscope data acquired from the CA1 region of the hippocampus in impaired animals. For example, we could use the miniscope data to compare the percentage of active cells during behavior, and during periods before and after behavior. Furthermore, we could analyze the sequences of neuron firing in the hippocampus during memory tasks. Both of these metrics cannot be measured using tetrode wire electrophysiology. It is worth noting that the miniscope cannot be used to collect LFP data from animals. It is for this reason that we have decided to focus on place cell spatial information data gathered from tetrode wire electrophysiology, since the miniscope would give us data that we could directly compare between the two techniques. Using this information, we sought to shed light on neuronal abnormalities in AD and paint a more complete picture on synaptic dysfunction and neuronal deficits during the early stages of AD.

CHAPTER 1: METHODS

Subjects

All animals used for the following experiments were approved for use by the Institutional Animal Care and Use Committee (IACUC) at the University of California San Diego (UCSD). All experiments were conducted under the guidelines outlined by the National Institutes of Health guidelines for the care and use of laboratory animals.

We used mouse models expressing the Swedish mutation (K670N/M671L) (Mullan et al., 1992) and the Indiana mutation (V717F) on APP (Murrell et al., 1991) to generate triple transgenic mouse models for AD that overexpress APP in the CA3 region of the hippocampus (CA3-APP mouse models). Animals were kept on a 12-hour light cycle, with animals being kept in a lit environment from 7AM until 7PM. Young animals were typically 4-6 months old, while aged animals were typically 16-18 months old. During behavior trials, animals were kept in regular light cycle conditions, but the light was dimmed in order to increase the comfort of the animals. Animals were kept at approximately 85% of baseline weight during the duration of the experiment and were fed water *ad libitum*. The food restriction was required in order to ensure that animals wouldeat the reward sugar pellets during the behavior task.

Habituation

Once ready for behavior, animals were brought up to the experiment room for several days in order to acclimate them to the novel environment. Once acclimated, animals were then allowed to begin several phases of the experiment. Furthermore, animals were handled for five to ten minutes during each acclimation day in order to become comfortable with researchers.

Note: Prior to every behavioral trial, animals were weighed to assess the health of the animal. Furthermore, the Figure 8 maze was wiped with Clorox disinfectant wipes in order to remove the smell of any animals that were previously on the maze. This allowed the animal to feel more comfortable on the maze, which greatly improved the efficiency of the behavior task.

Behavior: Phase 0

During this phase, animals were placed on the figure 8 maze for 10-15 minutes and allowed to run freely on the maze. Sugar pellets were dropped at several places on the maze and animals were allowed to eat freely on the maze. Once mice were comfortable with eating sugar pellets on the maze, they were moved to phase 1.

Behavior: Phase 1

During this phase, animals were put on the figure 8 maze, and forced to alternate from the right arm to the left in order to get the sugar. Animals were forced to continuously alternate on the maze for 15 minutes. Animals were not allowed to turn

around or run past the central arm of the maze. Once the animal could run in the forced alternation without being pushed, the animal moved to phase 2 of behavior training.

Behavior: Phase 2

During this phase, the animals were tasked with alternating between arms of the maze in order to find the sugar pellet (Figure 1). Animals were not forced to pick between arms of the maze; rather, animals were to remember which arm they ran through during the previous lap to pick the other arm for the subsequent lap. Animals were to run for 60 laps or for 20 minutes, whichever came first. Animals were still not allowed to turn around or run past the central arm, otherwise contact between the animal and researcher was minimal. After successfully having 80% or higher accuracy on which arm of the maze to pick for at least 4 out of the 5 last days of behavior, animals were allowed to move on to phase 3.

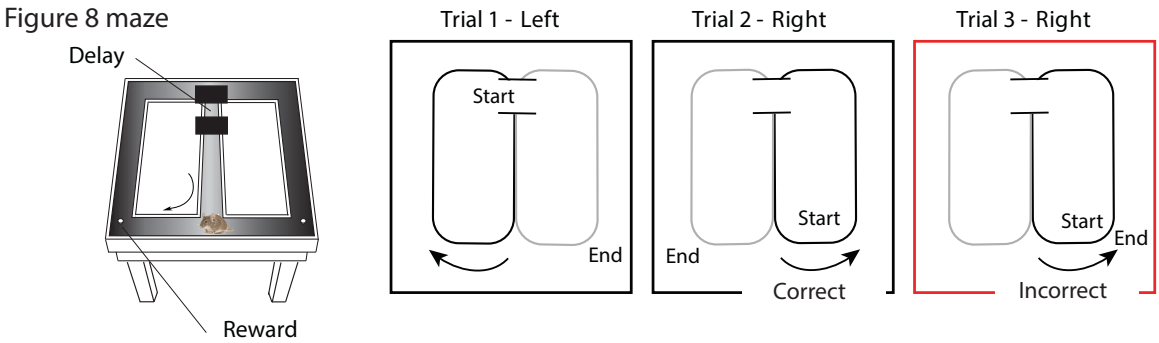

Figure 1. Figure 8 Spatial Memory Task. Animals were forced to alternate between the left and right sides of the maze in order to retrieve reward. Animals were allowed to "pass" to the next phase of the experiment when they reached percent accuracy of 80% or higher for 4 out of 5 days. Delays of 2 and 10 seconds were placed on the central arm of the maze in order to make the task hippocampal dependent.

Behavior: Phase 3

As with phase 2, animals were required to alternate between arms of the maze in order to retrieve the sugar pellet. Unlike phase 2 (which was hippocampus-independent), this phase incorporated a hippocampus-dependent spatial memory component. During the trial, the animal spent 10 laps without any delay (similar to phase 2), then spent 10 laps with a 2 second delay during the central arm, and later ran 10 more laps with a 10 second delay during the central arm (Figure 1). These delays were introduced through the use of barriers that entrapped the animals. These 30 laps were then repeated one more time during that day. It is important to note that the order of delays was scrambled every day in order to prevent the animal from getting used to the behavior task. After the animal completed the task for five days, the animal was then removed from food restriction, and prepared for the microdrive implant surgery.

Microdrive Implant Surgery

All surgeries were performed using aseptic procedures. Animals were anesthetized in a gas chamber filled with 4% isoflurane at 1L Oxygen/min, then moved to a Leica stereotaxic frame fitted with a nose cone at a constant influx of 2.5% isoflurane at 0.4L Oxygen/min (isoflurane levels were adjusted based on the weight and breathing rate of the animal). The animal was kept on a 37 degrees Celsius heating pad at all times during the surgery. Ophthalmic lubricant ointment was used to prevent eyes from dryness during the surgery. The heart rate and toe pinch reflex of the animals were both assessed prior to the start of the surgery and were assessed several times throughout the surgery. Once on the stereotaxic frame, the fur near the skull of the animals was shaved off. The

animals were then disinfected with saline and antiseptic povidone-Iodine solution three times. After being disinfected, a midline incision was made on the scalp of the animal using a scalpel blade. After opening up the skin, the animals were then given a subcutaneous injection of 0.1mL 2% lidocaine as a local anesthetic. Bregma was located on the skull and set to zero on the stereotaxic frame to align the animal. Once bregma was located, great care was taken to ensure that the skull of the animal was level both on the anterior-posterior axis, as well as the dorsal-lateral axis. If the axes had significant discrepancies, the axes were realigned to level the skull and the stereotaxic machine was zeroed again at bregma. Once aligned, a drill was moved 1.9mm down in the anterior-posterior axis and 1.85mm to the right in the medial-lateral axis. A small dent was made using the drill to signify the location of the microdrive implant. Next, 4-5 screws were added to the skull to stabilize the skull for microdrive implant. A hole was made first, and then each screw was inserted halfway into the hole, with the exception of one bigger hole that was made for the ground screw. Next, vetbond was added in order to seal the screws and the bone. Once the screws were in place, a craniotomy was performed at the site of the dent, where the bone was drilled until a thin flap remained. The flap was removed, exposing the dura, which was also subsequently removed. A drive was positioned at the center of this hole and inserted 0.3mm down from the surface of the brain in the dorsal-ventral axis. Neuroseal (2 drops Na_2 Alginate, 1 drop $CaCl_2$) was added to secure the drive into place. Finally, several layers of dental cement were added to further secure the drive as well as the screws. The animals were then injected with 0.05mg/kg - 0.1mg/kg of buprenorphine hydrochloride to act as a painkiller, before being placed in cages heated to 38 degrees Celsius to recover.

Spatial Memory Recording Protocol

Upon completion of the surgery, animals were allowed to rest for at least five days. After five days, animals were allowed to re-enter the room in order to habituate them to the room again. Over the course of the next several days, the animals were allowed to repeat phase 2 of the behavior, but with 30 laps instead of 60 laps in order to re-introduce the behavior task. Furthermore, this allowed the animals to adjust to running the behavior task while wearing the implanted microdrive. Great care was taken before the start of every behavior trial to ensure that the recording cable was not tangled and was the proper length (neither too tight nor too loose). Properly doing this before the start of any behavior or recording trial allowed for the animal to run comfortably through the maze, and greatly affected the behavior of the animal.

While habituating to the maze and becoming more comfortable with the cable, the tetrode wire on each microdrive unit was progressively turned lower until reaching a cell layer in the hippocampus. The wire first reached the CA1 region of the hippocampus, then the DG and CA3 regions of the hippocampus. During this time, the turning of the animal was limited to not more than 1/2 turns (226μM) per day (typically 1/8 (57μM) or 1/4 (113μM) per day until cell layer arrival). This was because the brain tissue offers resistance to the tetrode wire, meaning that it took time for the wire to penetrate the brain. We therefore waited, at minimum, several hours for the wire to stabilize in the new location of the brain. Furthermore, this strategy prevented us from overshooting the cell layer. Though the tetrode wire can be turned back up to find the cell layer, doing so would kill neurons in that layer, and therefore would affect the acquired results. Proper

arrival into the cell layer was defined by the presence of SWRs in the local field potential of the animal (LFP), as well as the presence of definable clusters.

Once the tetrode wire reached a cell layer for the animal, the animal began a recording protocol (Figure 2). Before recording, all channels on a microdrive were referenced to a quiet (non-noisy) channel without cells to subtract out baseline neuronal activity. This allowed for easy separation of cell clusters during analysis. The animal was first allowed to sleep in a box for ten minutes (15 minutes if recording from the CA3 region). Periods of sleep were defined as periods during which time, animals moved slower than 2 m/s. Next, animals were allowed to complete 30 laps of behavior in the same protocol as phase 3 behavior. During this time, we recorded the LFP, as well as individual cells from the animal, A camera at the ceiling of the room tracked the position of the animal using LED units on the microdrive unit to allow for correlation between cellular activity and spatial location. After the behavior task, the animal was allowed to sleep for 10 more minutes, during which time LFP and SWR activity was monitored again. This was then repeated more than one hour after the end of the task. This allowed us to ensure that the animal had completely stopped coding for spatial memory from the prior task. The animal was recorded from the same location in the cell layer one more time, then the tetrode was turned in order to record from different cell populations. After 10 days of recording, the animal was finished recording, and sacrificed for histological and immunohistochemical analysis.

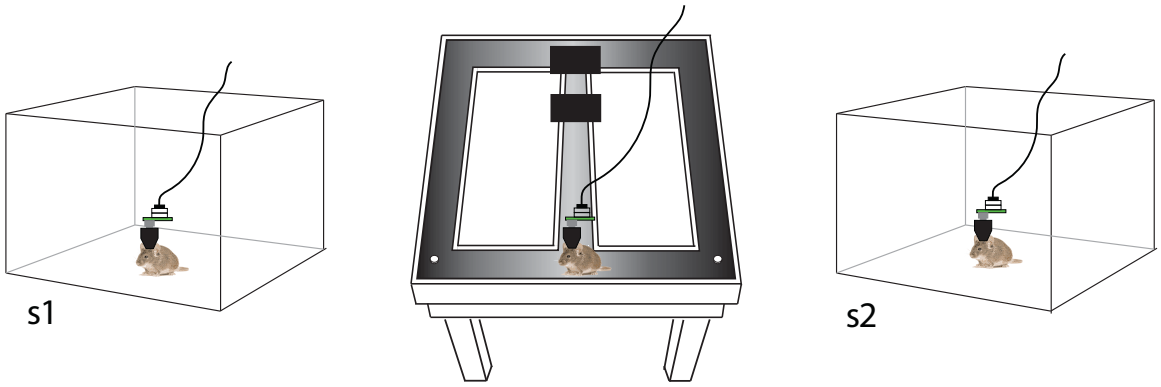

Figure 2. Spatial Memory Recording Protocol. Animals spent 10-15 minutes during "sleep" sessions before and after completing the spatial memory task. How long animals spent during sleep was dependent upon which cell layer recordings were taken from, where CA1 cells were recorded for 10 minutes per sleep, and CA3 cells were recorded for 15 minutes. Animals were defined as being quiet if they moved slower than 2 m/s.

Electrophysiology Recordings

Local Field Potential (LFP) and single unit recordings were collected using the implanted optetrode microdrive units. Electrode tips were plated with platinum to reduce electrical impedances to between 150-250 kΩ at 1kHz. A preamplifier, tether, and 16-channel data acquisition system (Neuralynx, Inc.) was used to record and collect all data for this experiment.

Perfusion and Tissue Preparation

Upon completion of the recording protocol, animals were anesthetized in a chamber filled with 5% isoflurane. The animals were then given a lethal injection of Sodium Pentobarbital (240mg/kg). The perfusion procedure then began after the animal was confirmed to be unresponsive to a toe pinch. The animals were perfused with Ringer solution (135mM NaCl, 5.4mM KCl, 1mM $MgCl_2 \cdot 6H_2O$, 1.8mM $CaCl_2 \cdot 2H_2O$, 5mM

HEPES) for five minutes, and then 4% Paraformaldehyde for approximately 3 minutes (total ~50mL of PFA used per animal). Once the perfusion was complete, the animal head was allowed to sit for an hour while PFA continued to fix surrounding brain tissue, thus allowing for the tetrode tracks to become well defined in the relevant hippocampal regions. The tetrode wires were slowly moved up and the brain was then carefully extracted from the skull and refrigerated at 4^{o}C in 4% PFA for 24 hours. After 24 hours, the brain was moved to 1X PBS solution and refrigerated.

The hippocampus of the animal was sectioned using a Leica vibratome. This was done by coronally sectioning 40 um slices. Half of all slices were stored in 1X PBS and mounted. The other half was stored in 0.02% Na-Azide and stored for immunohistochemical analysis.

APP Immunohistochemical Analysis

After sectioning, sections stored in 0.02% Na-Azide were rinsed 3 times for 5 minutes using 1X PBS. The sections were then incubated for 20 minutes in 400uL of 70% formic acid while shaking. The sections were rinsed again 3 times for 5 minutes using 1X PBS. Next, the sections were permeabilized with 300uL of solution containing 10% normal goat serum (NGS) and 0.5% Triton X-100 in 1X PBS. The sections were incubated for 90 minutes. Next, the sections were rinsed 3 times for 5 minutes using 2mL 1X PBS - 0.01% Triton X-100. The slices were then incubated for 24-30 hours in 250uL primary antibody. The primary antibody was diluted to 1:500 Primary antibody and consisted of 2% NGS and 0.01% Triton X-100 in 1X PBS. After the primary antibody incubation, slices were rinsed with about 2mL 1X PBS - 0.01% Triton X-100 3 times for

five minutes. The slices were then incubated for 2 hours (on a shaker) in 250uL of Secondary antibody solution. The secondary antibody solution was diluted to 1:1000 Secondary antibody and consisted of 0.01% Triton X-100 in 1X PBS. After the incubation, all slices were rinsed with about 2mL 1X PBS - 0.01% Triton X-100 3 times for five minutes. All slices were then incubated for 10 minutes in 300uL DAPI solution. The DAPI solution was a 1:5000 solution in 1X PBS. After incubation, slices were rinsed with 2mL 1X PBS 3 times for 5 minutes. The sections were then mounted with PBS, and coverslipped with Prolong Diamond Antifade at 20 degrees Celsius. The slices were stored in the dark until dry and were then imaged.

AAV-GCaMP7f Injection

All surgeries were performed using aseptic procedures. Animals were anesthetized in a gas chamber filled with 4% isoflurane at 1L Oxygen/min, then moved to a Leica stereotaxic frame fitted with a nose cone at a constant influx of 2.5% isoflurane at 0.4L Oxygen/min (isoflurane levels were adjusted based on the weight and breathing rate of the animal). The animal was kept on a 37 degrees Celsius heating pad at all times during the surgery. Ophthalmic lubricant ointment was used to prevent eyes from dryness during the surgery. The heart rate and toe pinch reflex of the animals were both assessed prior to the start of the surgery and were assessed several times throughout the surgery. Once on the stereotaxic frame, the fur near the skull of the animals was shaved off. The animals were then disinfected with saline and antiseptic povidone-Iodine solution three times. After being disinfected, a midline incision was made on the scalp of the animal using a scalpel blade. After opening up the skin, the animals were then given a

subcutaneous injection of 0.1mL 2% lidocaine as a local anesthetic. Bregma was located on the skull and set to zero on the stereotaxic frame to align the animal. Once bregma was located, great care was taken to ensure that the skull of the animal was level both on the anterior-posterior axis, as well as the dorsal-lateral axis. If the axes had significant discrepancies, the axes were realigned to level the skull and the stereotaxic machine was zeroed again at bregma. Once the stereotaxic machine was properly zeroed, a drill was moved to 2.1mm in the medial-lateral axis and -2.1mm on the anterior-posterior axis. The drill was then used to drill a hole through the skull and the dura and expose the surface of the brain. The drill was then replaced with a pipet filled with the AAV-GCaMP7f solution. The pipet was lowered to the surface of the brain, and then the stereotaxic frame was zeroed on the z-axis. The pipet was slowly lowered 1.35mm along the dorsal-ventral axis and 0.5uL of the AAV was slowly injected into the brain. After injection, the virus was allowed to dissipate for five minutes, before the pipet was raised out of the brain. The skin outside the skull was then sutured and disinfected with betadine. The animals were then injected with 0.05mg/kg - 0.1mg/kg of buprenorphine hydrochloride to act as a painkiller, before being placed in cages heated to 38 degrees Celsius to recover. After the surgery, animals were allowed to rest for 3 weeks while the virus expressed the GECI.

GRIN Lens Implant Surgery

All surgeries were performed using aseptic procedures. Animals were anesthetized in a gas chamber filled with 4% isoflurane at 1L Oxygen/min, then moved to a Leica stereotaxic frame fitted with a nose cone at a constant influx of 2.5% isoflurane at 0.4L Oxygen/min (isoflurane levels were adjusted based on the weight and breathing rate

of the animal). The animal was kept on a 37 degrees Celsius heating pad at all times during the surgery. Ophthalmic lubricant ointment was used to prevent eyes from dryness during the surgery. The heart rate and toe pinch reflex of the animals were both assessed prior to the start of the surgery and were assessed several times throughout the surgery. Once on the stereotaxic frame, the fur near the skull of the animals was shaved off. The animals were then disinfected with saline and antiseptic povidone-Iodine solution three times. Once disinfected, animals were given subcutaneous injections of 0.1 mL 2% lidocaine, 0.2mg/mL dexamethasone, and 5mg/Kg Carprofen. After being disinfected, a circular incision was made on the scalp of the animal using a sterilized scissors. Once the skull was exposed, the skull was cleaned with hydrogen peroxide. The neck muscles were then detached from the skull, and bleeding was allowed to stop. Bregma was then located on the skull and set to zero on the stereotaxic frame to align the animal. Once bregma was located, great care was taken to ensure that the skull of the animal was level both on the anterior-posterior axis, as well as the dorsal-lateral axis. If the axes had significant discrepancies, the axes were adjusted to level the surface of the skull and the stereotaxic machine was zeroed again at bregma. Once the stereotaxic frame was properly aligned, the injection site was verified, and six holes were drilled into the skull for anchor screws (1 on the left hemisphere, 2 on right frontal bone, and 3 in the occipital bone). The screws were then inserted, and blood was cleaned from the skull using cotton-tipped applicators. Super glue was then used to isolate borders of the skin, as well as fix the screws in the skull. Once the glue had dried, the site of the craniotomy was determined, and a small hole was softly drilled at that site. Next, the resulting piece of bone was removed without damaging the dura, and the surrounding skull was cleaned using 1X PBS. An aspiration

system was used with a 27G blunt needle and cold ringer solution. The cortex was slowly aspirated using the system (while being careful to avoid clogging of the needle due to dura), while cold ringer was applied in order to control bleeding. Aspiration was stopped once corpus callosum fibers became visible, and the needle was changed to the smaller 30G blunt needle that was then used to aspirate further cortex (white) until the Hippocampus (grey). Once the cortex was properly aspirated, several pipet tips were used to hold the GRIN lens in place at the center of the craniotomy hole. The stereotaxic frame was zeroed on the dorsal-ventral axis at the top of the skull, and the GRIN lens was slowly lowered 1.35mm (used primarily to visualize cells in the CA1 region of the hippocampus). Super glue was then used to hold the GRIN lens in place and was applied to the area surrounding the lens. Dental cement was then applied directly over the glue in order to allow the glue and the dental cement to cure together. After applying one more layer of dental cement, we verified that approximately 2mm of the GRIN lens was still visible at the top of the skull. Kwik-seal was then applied to the lens to prevent damage to the lens while the animals were in recovery.

After surgery, animals were injected with 0.3-0.5mL saline solution to accommodate blood loss. 0.25mg/mL Amoxicillin was added to all animals' water bottles for 7 days, and animals were given a subcutaneous injection of 0.2mg/kg dexamethasone and 5mg/kg carprofen for all 7 days. Upon the conclusion of the 7 days, animals were returned to a regular water bottle, and stopped receiving dexamethasone and carprofen injections.

Spike Sorting and Cell Classification

Spike sorting was performed using graphical cluster cutting software (MClust; A. D. Redish, University of Minnesota, Minneapolis) customized by Mankin et al. (2012). Spikes were clustered manually in two-dimensional projections of the multidimensional parameter space (consisting of waveform amplitudes, energies, and peak-to-valley ratios). Clusters persisting in the same region of parameter of space were accepted for analysis if spike waveform was distinct from noise signals. Additionally, autocorrelation functions were utilized to assist with identification of single units. Place cells were differentiated from interneurons based upon firing rate and peak to valley ratio (needed to have peak to valley ratio of 0.9 or greater).

Spatial Correlation

Spatial Correlation analysis was performed using methods outlined by Sabariego et al. (2019). The consistency of each cell's spatial firing pattern was measured by calculating, for each pair of left-turn trials and for each pair of right-turn trials, the Pearson's correlation between path segments at corresponding locations. Only correct trials were analyzed, and maze segments at the delay site were excluded. Pairwise comparisons in which the rates in all maze segments were less than 2 Hz were excluded. For each cell, the average correlation coefficient over all pairs of left-turn trials and the average over all pairs of right-turn trials was calculated, and the maximum of the two values was selected. The maximum was used so that cells with a place field on only one side of the maze would be assigned the correlation value from the trial type with the field. In addition to calculating spatial correlation coefficients between trials, we also averaged

the firing rates over all left-turn trials and over all right-turn trials. These averages were used to calculate the spatial correlation between corresponding segments on the right and left side of the figure-8 maze. Maze segments on the stem were excluded when calculating the correlation between the two sides.

Spatial Information

Spatial information was calculated for each cell as previously described (Skaggs et al., 1996):

$$\text{Spatial information} = \sum_i P_i \frac{\lambda_i}{\lambda} \log 2 \frac{\lambda_i}{\lambda},$$

where *i* is an index over spatial bins, Pi is the probability of the animal being in the *i*th bin, λi is the mean firing rate in the *i*th bin, and λ is the overall mean firing rate of the cell.

Statistical Analysis

All statistical analysis was performed using GraphPad Prism (Version 8). We wanted to focus on cells that were likely to have place fields, therefore we excluded every cell that did not have a peak firing rate of 2Hz in at least one spatial bin and had a mean firing rate lower than 5Hz. We used a D'Agostino-Pearson statistical test to evaluate whether the data sets were normally distributed. If the data set was normally distributed, then we used either a T-test, One-way ANOVA, or Two-way ANOVA to analyze the data. If the data was not normally distributed, we used a Kolmogorov-Smirnov test to analyze distributions, and a Mann-Whitney U test to analyze means.

CHAPTER 2: RESULTS

Immunohistochemical Analysis

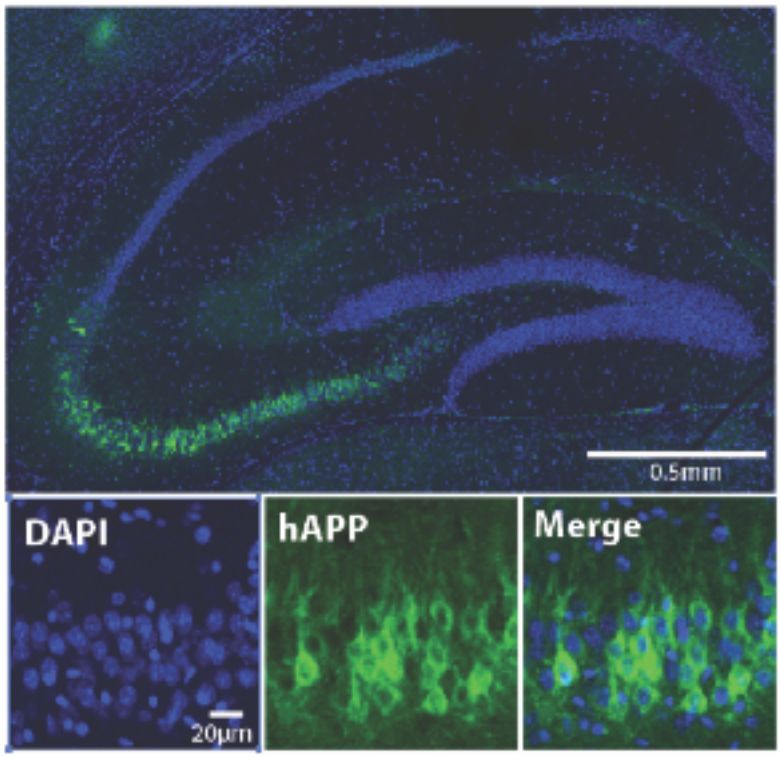

Figure 3. Immunohistochemistry Analysis Confirming APP Overexpression in Hippocampal CA3. Immunohistochemistry confirmed overexpression of APP in the hippocampal CA3 region (shown in green).

Immunohistochemistry showed that genetic overexpression of mutant human APP in the hippocampal region indeed led to the presence of APP expression that was limited to the target CA3 region without a leaky promoter (Figure 3). Approximately 60% of cells expressed APP at 4-6 months old, while about 80% of cells expressed the mutant form of APP when 16-18 months old.

CA3-APP Behavior Impairments

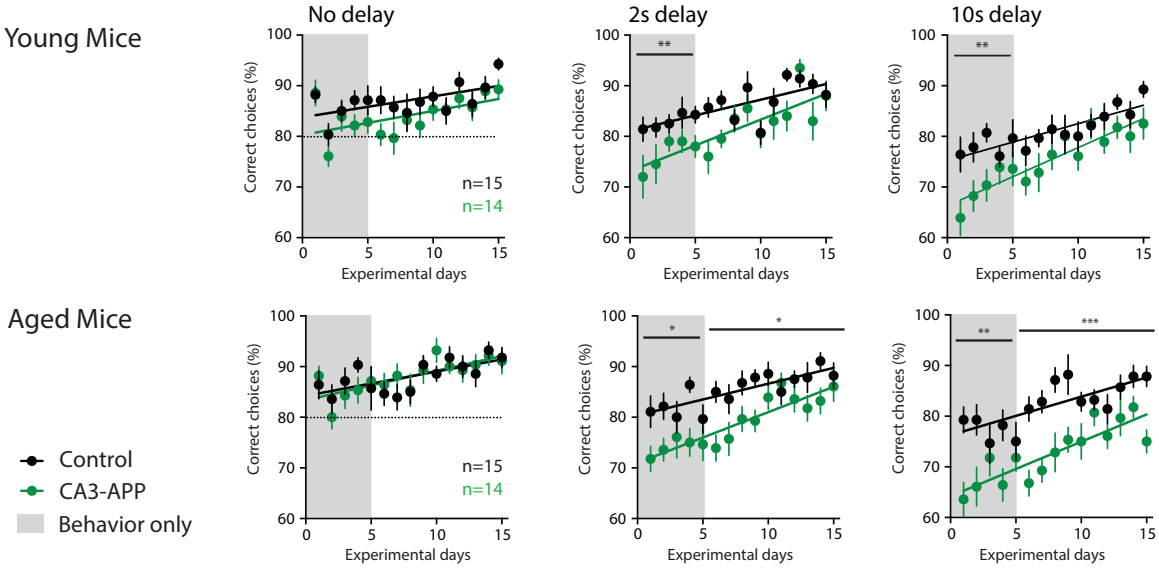

Figure 4. CA3-APP animals show significant behavioral deficits during a hippocampus-dependent memory task. Regression analysis of percentage correct alternation frequency of both young and aged control (black) and CA3-APP animals (green) without delay, with a 2 second delay, and with a 10 second delay during the figure 8 spatial memory task. Young CA3-APP animals showed significant impairments in percent accuracy during the 2 and 10 second delays before surgery ($p<0.01$ and $p<0.01$, respectively), while aged CA3-APP animals showed significant impairments in percent accuracy during the 2 and 10 second delay, even after surgery ($p<0.05$, $p<0.05$ – d2; $p<0.01$, $p<0.001$ – d10).

First, we conducted behavior analysis of CA3-APP animals to show that the spatial memory task with delays was indeed hippocampal dependent (Figure 4). Behavior analysis of aged and young CA3-APP animals and control animals showed that young animals had significant decreases in correct choice frequency during the 2 and 10 second delays prior to surgery ($p<0.01$ and $p<0.01$, respectively). Aged CA3-APP animals showed a significant decrease in percent correct choices during the 2 and 10 second delay both before and after surgery ($p<0.05$, $p<0.05$ – d2; $p<0.01$, $p<0.001$ – d10). That being

said, all animals showed improvements in behavior, where CA3-APP animals showed improvement at the same rate as control animals (but seldom reaching percent accuracy of control animals). Aged animals showed improvement at a lower rate than young animals, where young animals did not show statistically significant differences relative to control after at least 5 days of training.

Histological Tetrode Tracking Analysis

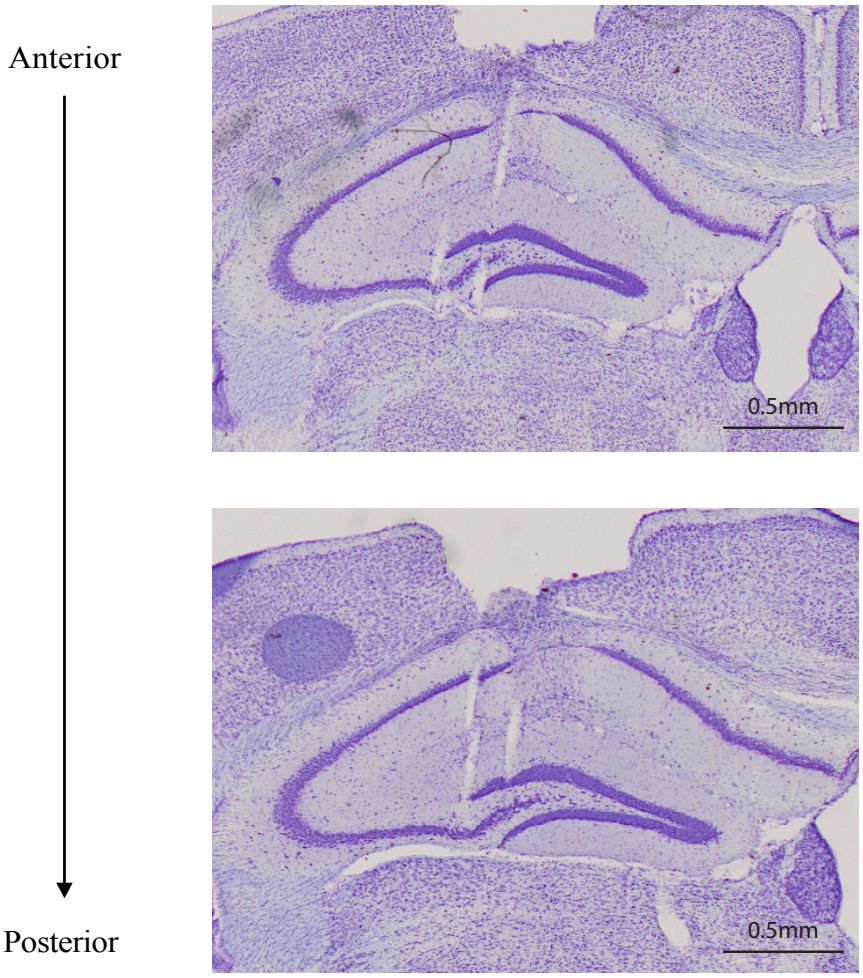

Figure 5. Tetrode tracking analysis of Microdrive implant. Histological analysis of extracted brains at 40uM slices confirms presence of tetrode tracks in the target CA1 and CA3/DG regions of the hippocampus. Turning mechanism of Microdrive allows for tetrode wires to descend into deeper layers of the hippocampus.

Histological analysis of animals following Microdrive implant confirms the presence of tetrode tracks in the target CA1 and CA3 regions of the hippocampus (Figure 5). The turning mechanism of the Microdrive allowed for selective turning of the tetrode wires to deeper layers of the hippocampus. This histological analysis confirmed that our

data sets were acquired from the right regions of the hippocampus and set the stage for all further analysis.

Hippocampal Place Cell Dysfunction

We began our analysis by looking at place cell dysfunction in the form of altered mean and peak firing rates in young and aged CA3-APP animals vs. control animals. For mean and peak firing rate of both CA1 and CA3 neurons, we did not exclude any cells with peak firing rates below 2Hz, thereby including neurons other than place cells in the analysis. Mean firing rate consisted of analyzing the mean firing rate of any particular cell at any point during the memory task, while peak firing rate analyzed the maximal firing rate of a cell at any point during the task.

Analysis of mean and peak firing rates of CA1 place cells in aged CA3-APP animals and control animals as well as in young CA3-APP animals and control animals showed that CA1 place cells in young CA3-APP animals did not have significant differences in mean of mean firing rates or in distribution of mean firing rates ($p>0.05$, Mann Whitney U test, KS test) (Figure 6A) but had lower mean peak firing rates during the 10 second delay ($p<0.01$, Mann Whitney U test) (Figure 6C). The mean of the mean firing rates of CA1 place cells in young CA3-APP animals was 1.239Hz ± 0.08066Hz during d0 (N=351) and 1.180Hz ± 0.07704Hz during d10 (N=350) (Figure 6A). The mean of the mean firing rates of CA1 place cells in young control animals was 1.401Hz ± 0.0705Hz during d0 (N=590) and 1.464Hz ± 0.07704Hz during d10 (N=592) (Figure 6A). The mean peak firing rate of CA1 place cells in young CA3-APP animals was 13.08Hz ± 0.6827Hz during d0 and 12.20Hz ± 0.6329Hz during d10 (Figure 6C). The

mean peak firing rate of CA1 place cells in young control animals was 15.33Hz ± 0.6422Hz during d0 and 15.32Hz ± 0.5875Hz during d10 (Figure 6C). KS tests of CA1 place cell mean and peak firing rate distributions during all delay conditions in aged animals showed significant differences between peak firing rates of young CA3-APP animals and control animals, but did not show a statistically significant difference between distribution of mean firing rate ($p<0.01$, KS test) (Figure 6A, 6C). Both mean and peak firing rates did not change as the task became more hippocampal dependent.

In the aged group, CA3-APP animals did not show significantly lower CA1 place cell mean firing rates through all delay conditions ($p>0.05$, Mann Whitney U test. The means of the mean firing rates of CA1 place cells in aged CA3-APP animals were 0.9049Hz ± 0.05083Hz during d0 (N=659) and 0.8962Hz ± 0.04758Hz during d10 (N=654) (Figure 6B). The means of the mean firing rates in aged control animals were 1.090Hz ± 0.05506Hz during d0 (N=730) and 1.092Hz ± 0.05325Hz during d10 (N=706) (Figure 6B). The mean peak firing rates of CA1 place cells in aged CA3-APP animals were 10.81Hz ± 0.4724Hz during d0 (N=659) and 10.32Hz ± 0.4319Hz during d10 (N=654) (Figure 6D). Mean peak firing rates of CA1 place cells in aged control animals were 13.51Hz ± 0.5643Hz during d0 (N=713) and 12.87Hz ± 0.5297Hz during d10 (N=706). KS tests of CA1 place cell mean and peak firing rate distributions during all delay conditions in young animals showed significant differences between CA3-APP animals and control animals ($p<0.001$, Figure 6B; $p<0.01$ Figure 6D; KS test). Neither mean nor peak firing rates changed as the task became more hippocampal dependent.

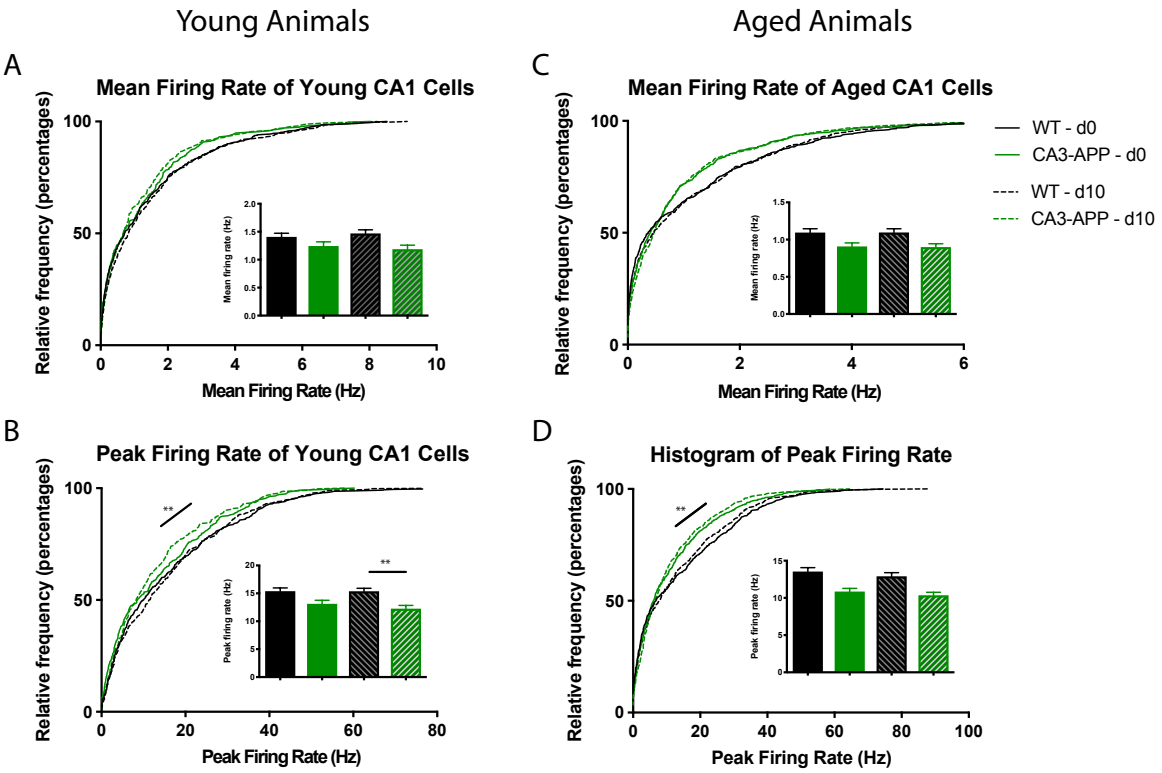

Figure 6. Mean Firing Rates of CA1 Place Cells in Young and Aged Control vs. CA3-APP animals. (A) Mean firing rate of CA1 cells in young animals compared between control and CA3-APP animals across 0 and 10 second delays. (B) Mean firing rate of CA1 cells in young animals compared between control and CA3-APP animals across 0 and 10 second delays. (C) Peak firing rate of CA1 cells in aged animals compared between control and CA3-APP animals across 0 and 10 second delays. (D) Peak firing rate of CA1 cells in aged animals compared between control and CA3-APP animals across 0 and 10 second delays. Significance (* = $p<0.05$, ** = $p<0.01$) of distributions was evaluated using a KS test, while significance of means was evaluated using a Mann Whitney U test. Error bars represent one standard error away from mean.

Next, we analyzed mean and peak firing rates of CA3 place cells in CA3-APP animals. The mean of the mean firing rates of CA3 place cells in young CA3-APP animals was 0.8560Hz ± 0.05011Hz during d0 (N=628) and 0.8580Hz ± 0.05112Hz (N=630) during d10 (Figure 7A). The mean peak firing rates of CA3 place cells in young CA3-APP animals was 12.36Hz ± 0.5948Hz during d0 and 12.12Hz ± 0.59364Hz during

d10 (Figure 7C). The mean of the mean firing rates of CA3 place cells in young control animals was 0.6995Hz ± 0.07972Hz during d0 (N=315) and 0.7362Hz ± 0.07942Hz (N=315) during d10 (Figure 7B). The mean peak firing rates of CA3 place cells in young control animals were 9.857Hz ± 0.9797Hz during d0 and 10.07 Hz ± 0.9408Hz during d10 (Figure 7C). KS tests of CA3 place cell mean and peak firing rate distributions during all delay conditions in young animals showed significant decreases in CA3-APP mean and peak firing rate relative to control ($p<0.001$, KS test; Figure 7A,7C). Both mean and peak firing rates did not change as the task became more hippocampal dependent.

In the aged group, CA3-APP animals did not show statistically significant differences in mean firing rate across all delay conditions ($p>0.05$, Mann-Whitney U test), but a statistically significant difference in peak firing rate distribution ($p<0.01$, KS test). The mean of the mean firing rates of CA3 place cells in aged CA3-APP animals was 0.8495Hz ± 0.05284Hz during d0 (N=472) and 0.8925Hz ± 0.06726Hz during d10 (N=312) (Figure 7B). The mean of the mean firing rates of CA3 place cells in aged control animals was 0.8791Hz ± 0.04743Hz during d0 (N=730) and 0.8918Hz ± 0.05083Hz during d10 (N=500) (Figure 7B). The mean peak firing rates of CA3 place cells in aged CA3-APP animals was 10.28Hz ± 0.5452Hz during d0 (N=412) and 10.62 ± 0.6550Hz during d10 (N=312) (Figure 7D). The mean peak firing rates of CA3 place cells in control animals were 13.68Hz ± 0.6236Hz during d0 (N=713) and 13.15 ± 0.6743Hz during d10 (N=500) (Figure 7D). KS tests of CA3 place cell mean and peak firing rate distributions during all delay conditions in young animals showed significant

increases in mean and peak firing rate of CA3-APP animals relative to control animals for peak firing rate, but not for mean firing rate, while aged CA3-APP animals showed greater distribution of lower firing rate relative to control ($p<0.01$, KS test; Figure 7B, 7D). The means of both mean and peak firing rates between control and CA3-APP animals were not significant in aged animals ($p>0.05$, Mann-Whitney U test). Neither mean nor peak firing rates changed as the task became more hippocampal dependent.

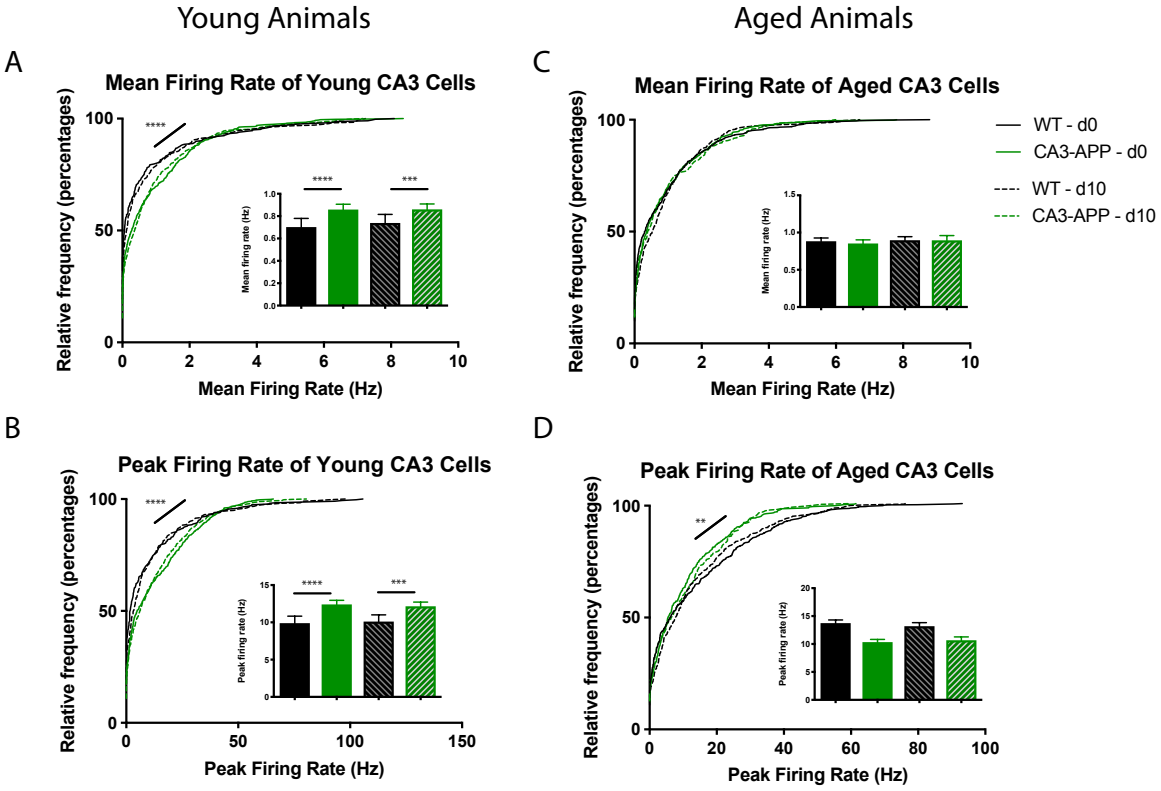

Figure 7. Firing Rates of CA3 Place Cells in Young and Aged Control vs. CA3-APP animals. (A) Mean firing rate of CA3/DG cells in young animals compared between control and CA3-APP animals across 0 and 10 second delays. (B) Mean firing rate of CA1 cells in aged animals compared between control and CA3-APP animals across 0 and10 second delays. (C) Peak firing rate of CA1 cells in young animals compared between control and CA3-APP animals across 0 and 10 second delays. (D) Peak firing rate of CA1 cells in aged animals compared between control and CA3-APP animals across 0 and 10 second delays. Significance (** = $p<0.01$, *** = $p<0.001$, **** = $p<0.0001$) of distributions was evaluated using a KS test, while significance of means was evaluated using a Mann Whitney U test. Error bars represent one standard error away from mean.

Next, we looked at information score and across sides correlation of both CA3 and CA1 place cells in CA3-APP animals. We compared information score and across sides correlation spatial information metrics between CA1 place cells in aged CA3-APP animals and control animals as well as in young CA3-APP animals and control animals. Information score was used as a metric evaluating how scattered the firing of a cell is during the memory task. If a place cell is less impaired, it should code a higher information score and have more precise firing in a target area of the maze. Furthermore, across sides correlation evaluates how likely a place cell is to fire in an identical arm of the maze in a different spatial location. An unimpaired place cell should be able to discriminate easily between the two arms, and therefore have lower across sides correlation.

We found that, as the delay period increased on the figure 8 spatial memory task, all animals showed decreases in information score, regardless of genotype ($p<0.05$, KS test). The mean information scores for CA1 place cells in young CA3-APP animals were 1.444 ± 0.04425 for young animals during d0 (N=273), and 1.164 bits/sec $\pm$ 0.04538 bits/sec during d10 (N=288) (Figure 8A). The mean information scores for CA1 place cells in young control animals were 1.573 bits/sec $\pm$ 0.03715 bits/sec for young animals during d0 (N=498), and 1.136 bits/sec $\pm$ 0.03988 bits/sec during d10 (N=500) (Figure 8A). The mean information scores of CA1 place cells in young CA3-APP animals relative to control were significantly decreased during d10 ($p<0.05$, Mann Whitney U Test). Distribution of information scores of CA1 place cells was statistically significantly different during d10 in young animals ($p<0.01$, KS test). Furthermore, aged animals

displayed a statistically significant decreases between CA1 place cell information scores distributions of control and CA3-APP animals ($p<0.01$, KS test), where the difference was most pronounced during the 10 second delay period. The mean information scores of CA1 place cells in aged CA3-APP animals were 1.558 bits/sec ± 0.03751 bits/sec during d0 (N=477), and 1.306 bits/sec ± 0.03786 bits/sec during d10 (N=512) (Figure 8B). The mean information scores of CA1 place cells in aged control animals were 1.721 bits/sec ± 0.04218 bits/sec during d0 (N=506), and 1.523 bits/sec ± 0.04840 bits/sec during d10 (N=513) (Figure 8B). Mean information scores of CA1 place cells in aged control vs. CA3-APP animals were statistically significantly decreased during both d0 and d10 ($p<0.05$, $p<0.01$; Mann Whitney U-Test). Next, the mean across sides correlation for CA1 place cells in CA3-APP animals was 0.07560 ± 0.01977 for young animals during d0 (N=265), and 0.2507 ± 0.02350 during d10 (N=286) (Figure 8C). The mean across sides correlations for CA1 place cells in young control animals was 0.1012 ± 0.01531 during d0 (N=433), and 0.1600 ± 0.01656 during d10 (N=486) (Figure 8C). The mean across sides correlations of CA1 place cells in aged CACA3-APP animals were 0.1187 ± 0.01595 during d0 (N=443), and 0.1654 ± 0.01604 during d10 (N=490) (Figure 8D). The mean across sides correlation of CA1 place cells in aged control animals was 0.08084 ± 0.01492 during d0 (N=444), and 0.1662 ± 0.01653 during d10 (N=482) (Figure 8D). The mean across sides correlations for CA3-APP young animals versus control young animals was statistically significantly higher during d10 ($p<0.01$, Mann-Whitney U Test). The distribution of across sides correlation of young CA3-APP animals versus control were also statistically significant higher ($p<0.05$, KS test). Aged CA3-APP animals showed

statistically significant increases in CA1 place cell spatial correlation relative to control ($p<0.05$, KS test).

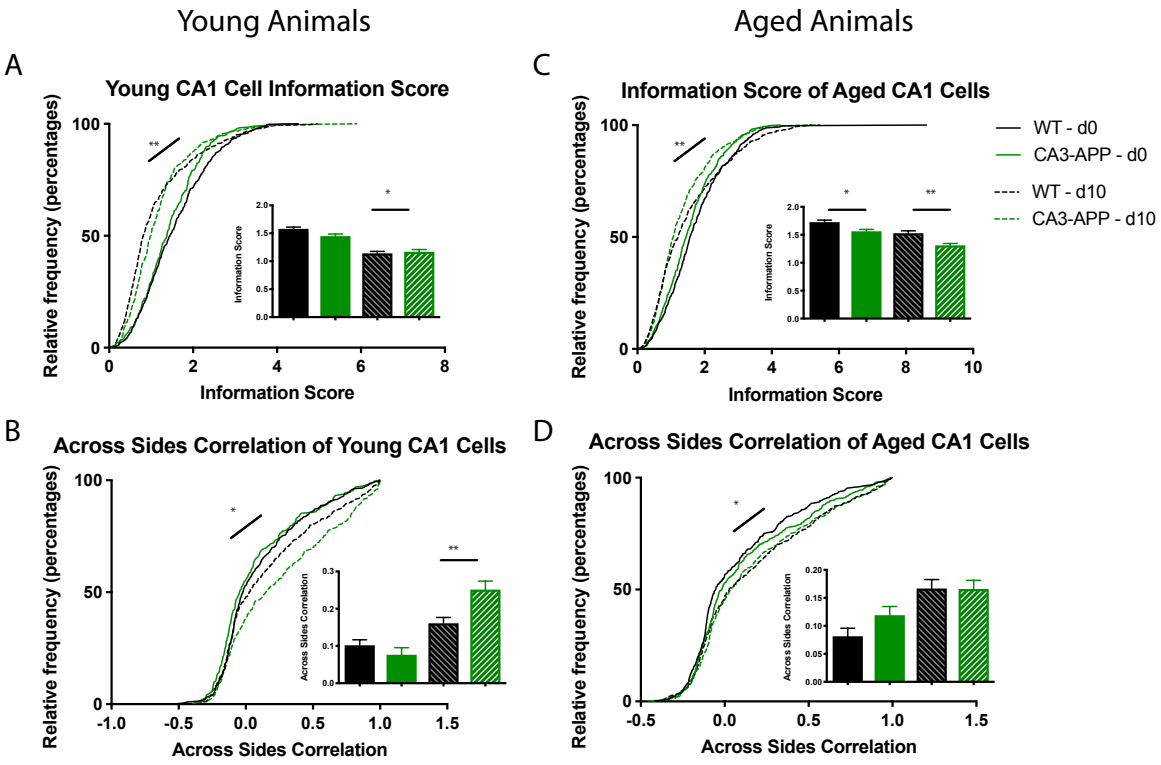

Figure 8. Spatial Information of CA1 Place Cells in Young and Aged Control vs. CA3-APP animals. (A) Information score (bits/sec) of CA1 cells in young animals compared between control and CA3-APP animals across 0 and 10 second delays. (B) Information score (bits/sec) of CA1 cells in aged animals compared between control and CA3-APP animals across 0 and 10 second delays. (C) Across sides correlation of CA1 cells in young animals compared between control and CA3-APP animals across 0 and 10 second delays. (D) Across sides correlation of CA1 cells in aged animals compared between control and CA3-APP animals across 0 and 10 second delays. Significance (* = $p<0.05$, ** = $p<0.01$) of distributions was evaluated using a KS test, while significance of means was evaluated using a Mann Whitney U test. Error bars represent one standard error away from mean.

Next, we compared information score and across sides correlation spatial information metrics between CA3/DG place cells in aged CA3-APP animals and control animals as well as in young CA3-APP animals and control animals. The mean

information scores for CA3 place cells in CA3-APP animals were 1.768 bits/sec ± 0.04319 bits/sec for young animals during d0 (N=399), and 1.408 bits/sec ± 0.04075 bits/sec during d10 (N=407) (Figure 9A). The mean information scores for CA3 place cells in young control animals were 1.941 bits/sec ± 0.06080 bits/sec during d0 (N=251), and 1.623 bits/sec ± 0.07222 bits/sec during d10 (N=276) (Figure 9A). The mean information scores of CA3 place cells between young CA3-APP animals and control were significantly lower during d0 ($p<0.01$, Mann Whitney U Test). Distribution of information scores of CA3 place cells was statistically significantly different during d10 in young animals ($p<0.01$, KS test). Furthermore, aged animals displayed a statistically significant difference between CA3 place cell information scores distributions of control and CA3-APP animals ($p<0.0001$, KS test), where the difference was most pronounced during the 10 second delay period. The mean information scores of CA3 place cells in aged CA3-APP animals were 1.440 bits/sec ± 0.04343 bits/sec during d0 (N=336), and 1.201 ± 0.05086 during d10 (N=206) (Figure 9B). The mean information scores of CA3 place cells in aged control animals were 1.828 bits/sec ± 0.04205 bits/sec during d0 (N=506), and 1.387 bits/sec ± 0.04888 bits/sec during d10 (N=369) (Figure 9B). Mean information scores of young control vs CA3-APP animals were statistically significantly lower in CA3-APP animals during d0 and d10 ($p<0.0001$, $p<0.05$; Mann Whitney U-Test). Next, there was a decrease in mean spatial correlation for CA3 place cells in young control animals ($p<0.05$, Mann Whitney U test test) during the 10 second delay period, as well as a significant decrease in the distribution of across sides correlations ($p<0.05$, KS test). The mean across sides correlations of CA3 place cells in young CA3-APP animals

were 0.08836 ± 0.01654 during d0 (N=356), and 0.1383 ± 0.01695 during d10 (N=400) (Figure 9C). The mean across sides correlations of CA3 place cells in young control animals were 0.1092 ± 0.02350 during d0, and 0.2294 ± 0.02412 during d10 (N=253) (Figure 9C). The mean across sides correlations of CA3 place cells of CA3-APP young animals versus control young animals was statistically significantly lower during d10 ($p<0.01$, Mann-Whitney U Test). The distribution of across sides correlation was statistically significantly lower for young CA3-APP animals during d10 ($p<0.05$, KS test). Next, aged animals displayed increases in both the distribution and the mean of across sides correlation of CA3 place cells during the 10 second delay, where CA3-APP animals showed statistically significant increases in spatial correlation relative to control ($p<0.05$, KS test, Mann Whitney U test). The mean across sides correlations of CA3 place cells for aged CA3-APP animals were 0.1075 ± 0.01699 for aged animals during d0 (N=323), and 0.2453 ± 0.02808 during d10 (N=199) (Figure 9D). The mean across sides correlations for CA3 place cells in control aged animals were 0.09130 ± 0.01534 for aged animals during d0, and 0.1591 ± 0.01873 during d10 (N=345) (Figure 9D). The mean across sides correlation of CA3-APP aged animals versus control aged animals was statistically significantly higher during d10 ($p<0.05$, Mann-Whitney U Test). The distribution of across sides correlations between CA3-APP aged animals and control aged animals was statistically significantly lower during d10 ($p<0.05$, KS test).

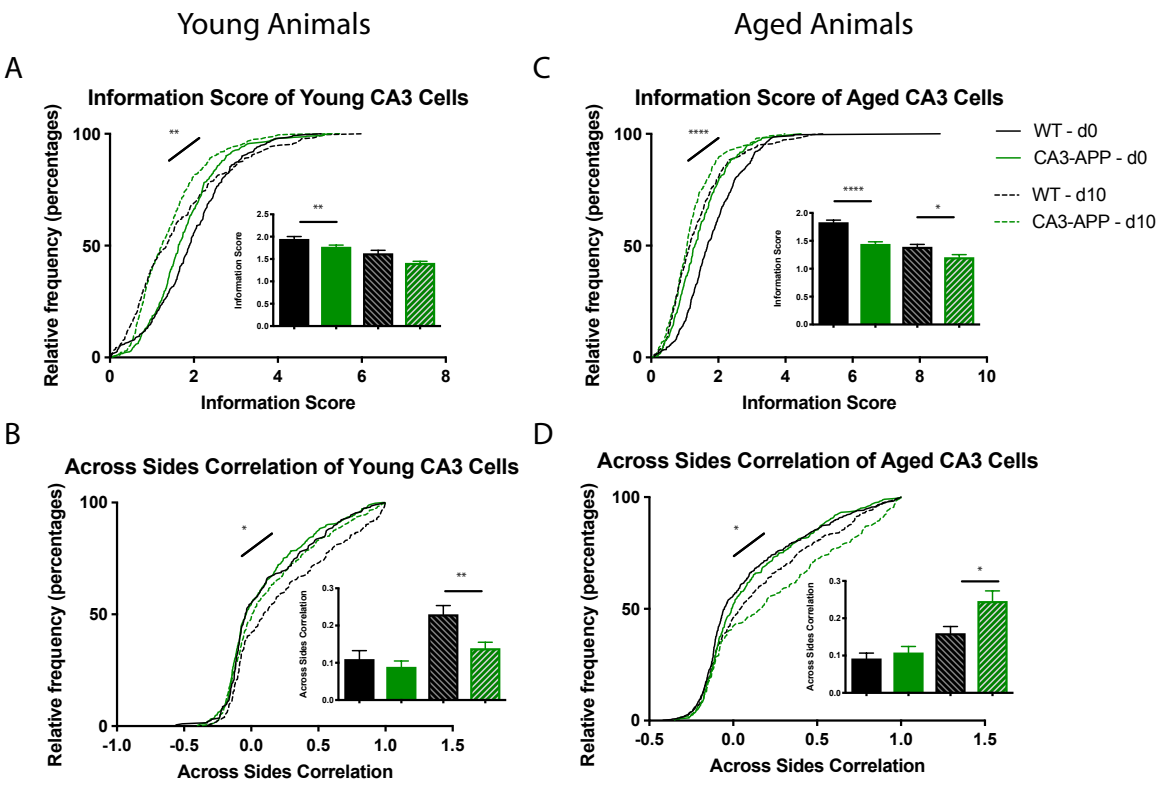

Figure 9. Spatial Information of CA3 Place Cells in Young and Aged Control vs. CA3-APP animals. (A) Information score (bits/sec) of CA3/DG cells in young animals compared between control and CA3-APP animals across 0 and 10 second delays. (B) Information score (bits/sec) of CA3/DG cells in aged animals compared between control and CA3-APP animals across 0 and 10 second delays. (C) Across sides correlation of CA3/DG cells in young animals compared between control and CA3-APP animals across 0 and 10 second delays. (D) Across sides correlation of CA3/DG cells in aged animals compared between control and CA3-APP animals across 0 and 10 second delays. Significance (* = $p<0.05$, ** = $p<0.01$, **** = $p<0.0001$) of distributions was evaluated using a KS test, while significance of means was evaluated using a Mann Whitney U test. Error bars represent one standard error away from mean.

After completing analysis on firing rate, information score, and across sides correlation metrics, we next evaluated trial by trial stability of place cell activation in CA1 and CA3/DG cells of young and aged CA3-APP animals and controls. Trial by trial stability of place cells evaluated how likely a place cell was to fire in the exact same location once the animal ran through it during the task. Higher stability meant that the

place cell was more likely to fire in that location every time the animal ran through that section of the maze.

For young CA3-APP animals, mean trial by trial correlation for CA1 cells was found to be 0.5502 ± 0.01606 during d0 (N=271), and 0.5830 ± 0.01522 during d10 (N=287). For young control animals, mean trial by trial correlation for CA1 cells was found to be 0.5418 ± 0.01263 during d0 (N=492), and 0.5598 ± 0.01156 during d10 (N=497) (Figure 10A). For young CA3-APP animals, mean trial by trial correlation for CA3 cells was found to be 0.5512 ± 0.01991 during d0 (N=196), and 0.5484 ± 0.01879 during d10 (N=205). For young control animals, mean trial by trial correlation for CA3 cells was found to be 0.5793 ± 0.01328 during d0 (N=495), and 0.5206 ± 0.01431 during d10 (N=365) (Figure 10B). For aged CA3-APP animals, mean trial by trial correlation for CA1 cells was found to be 0.5947 ± 0.01222 during d0 (N=476), and 0.5676 ± 0.01220 during d10 (N=506). For aged control animals, mean trial by trial correlation for CA1 cells was found to be 0.5930 ± 0.01253 during d0 (N=497), and 0.6069 ± 0.01178 during d10 (N=509) (Figure 10C). For aged CA3-APP animals, mean trial by trial correlation for CA3 cells was found to be 0.5467 ± 0.01451 during d0 (N=332), and 0.5484 ± 0.01879 during d10 (N=205). For aged control animals, mean trial by trial correlation for CA3 cells was found to be 0.5793 ± 0.01328 during d0 (N=495), and 0.5206 ± 0.01431 during d10 (N=365) (Figure 10D). No statistically significant differences were found between trial by trial stability in young CA3-APP and control animals. In aged CA3-APP animals, CA1 cells showed statistically significant decreases in distribution and mean of trial by trial correlation during d10 ($p<0.05$, KS test, Mann Whitney U test). In aged CA3-APP

animals, CA3 cells showed statistically significant decreases in distribution and mean of trial by trial correlation during d0 ($p<0.001$, KS test; $p<0.05$, Mann Whitney U test).

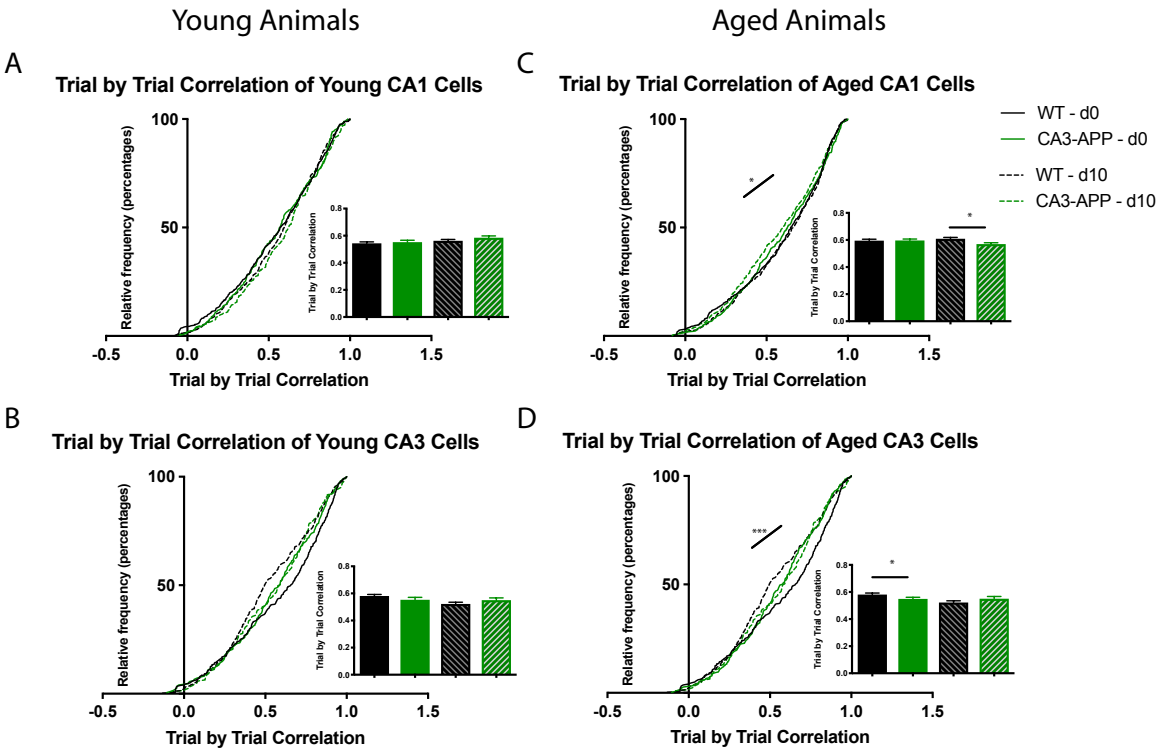

Figure 10. Trial by Trial Correlation of CA1 and CA3 Place Cells in Young and Aged Control vs. CA3-APP animals. (A) Trial by trial correlation of CA1 cells in young animals compared between control and CA3-APP animals across 0 and 10 second delays. (B) Trial by trial correlation of CA3/DG cells in young animals compared between control and CA3-APP animals across 0 and 10 second delays. (C) Trial by trial correlation of CA1 cells in aged animals compared between control and CA3-APP animals across 0 and 10 second delays. (D) Trial by trial correlation of CA3/DG cells in aged animals compared between control and CA3-APP animals across 0 and 10 second delays. Significance (* = $p<0.05$, *** = $p<0.001$) of distributions was evaluated using a KS test, while significance of means was evaluated using a Mann Whitney U test. Error bars represent one standard error away from mean.

Finally, we compared place field size in young and aged CA3-APP animals and control animals during all delays of the task. Place field size was indicative of place cell precision during the task. Smaller place field size meant that place cells were firing when

coding for specific locations, while larger place fields would have indicated less precise place cell coding of spatial location.

Mean place field size of CA1 place cells in young CA3-APP animals was 14.33 ± 0.5080 (N=218) and 12.14 ± 0.3168 (N=380) in control animals (Figure 11A). Mean place field size of CA1 place cells in aged CA3-APP animals was 12.87 ± 0.3971 (N=357) and 11.95 ± 0.3176 (N=407) in control animals (Figure 11B). Mean place field size of CA3 place cells in young CA3-APP animals was 14.33 ± 0.5080 (N=218) and 12.14 ± 0.3168 (N=380) in control animals (Figure 11C). Mean place field size of CA3 place cells in aged CA3-APP animals was 13.79 ± 0.5470 (N=237) and 9.686 ± 0.2438 (N=431) in control animals (Figure 11D). KS tests of all four distributions showed that CA3-APP animals have significantly increased distributions of higher place fields for CA1 and CA3 cells in both young and aged animals ($p<0.01$).

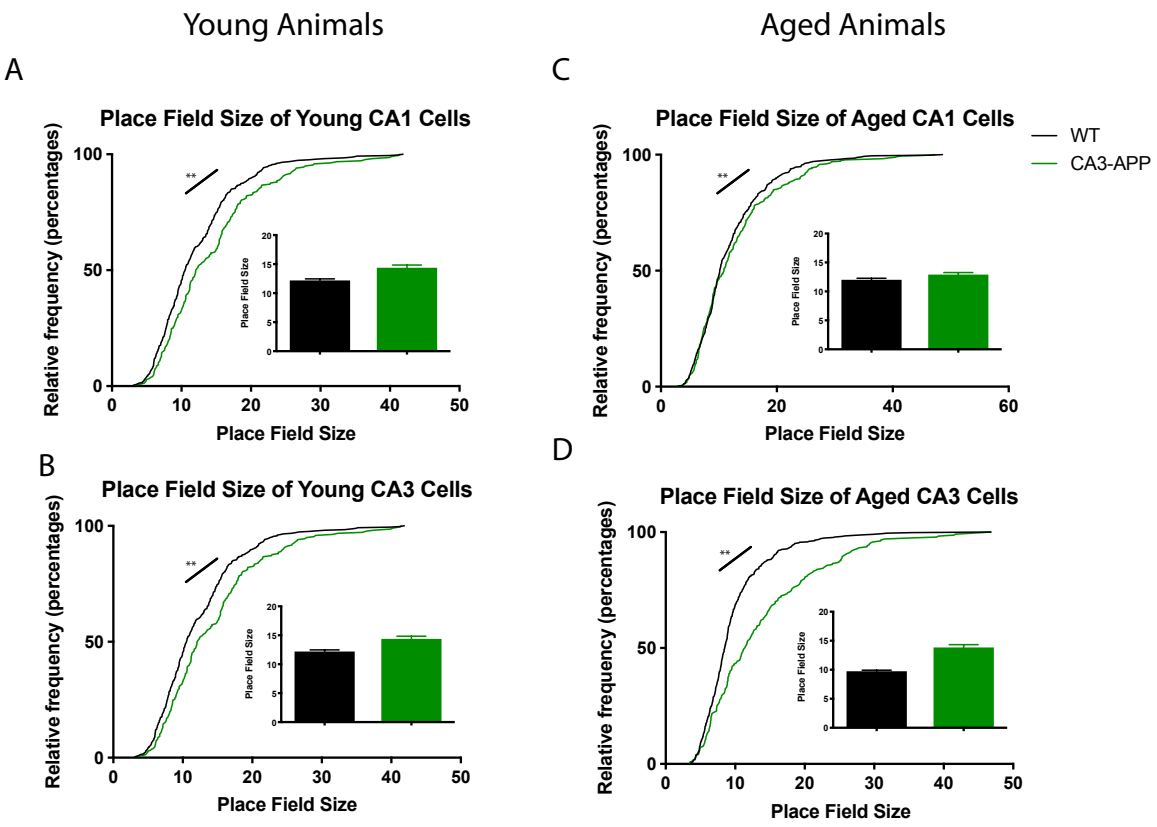

Figure 11. Place Field Size of CA1 and CA3 Place Cells in Young and Aged CA3-APP Animals Relative to Control. (A) Place field size of CA1 place cells during all delays of the task in young CA3-APP animals relative to control. (B) Place field size of CA3/DG place cells during all delays of the task in young CA3-APP animals relative to control. (C) Place field size of CA1 place cells during all delays of the task in aged CA3-APP animals relative to control. (D) Place field size of CA3 place cells during all delays of the task in aged CA3-APP animals relative to control. Significance (** = $p<0.01$) of distributions was evaluated using a KS test, while significance of means was evaluated using a Mann Whitney U test. Error bars represent one standard error away from mean.

Calcium Imaging

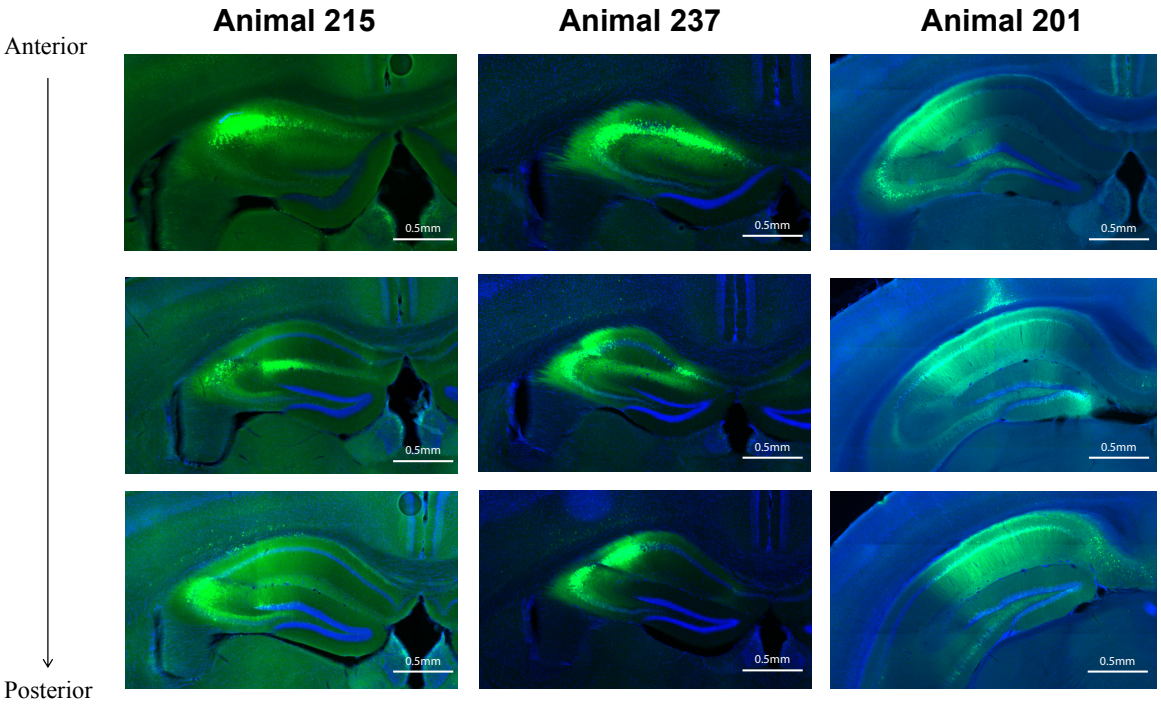

Figure 12. Histological analysis of GCaMP7f-GECI expression. Histological analysis of extracted brains at 60uM slices confirms expression of GCaMP7f GECI in target CA1 region of the hippocampus.

Before implanting the GRIN lens, we first confirmed that viral injection of AAV-GCaMP7f indeed led to visualization of the GFP fluorophore in target regions of the hippocampus. Histological analysis of GCaMP7f expression confirmed expression of GECI in the target CA1 region of the hippocampus (Figure 12). It is important to note, however, that posterior sections of the brain began showing expression in the CA2 region of the hippocampus. Further injections were adjusted to prevent this and only show expression in the CA1 region. This was done primarily by adjusting where bregma was located to zero the stereotaxic frame slightly more anterior than before.

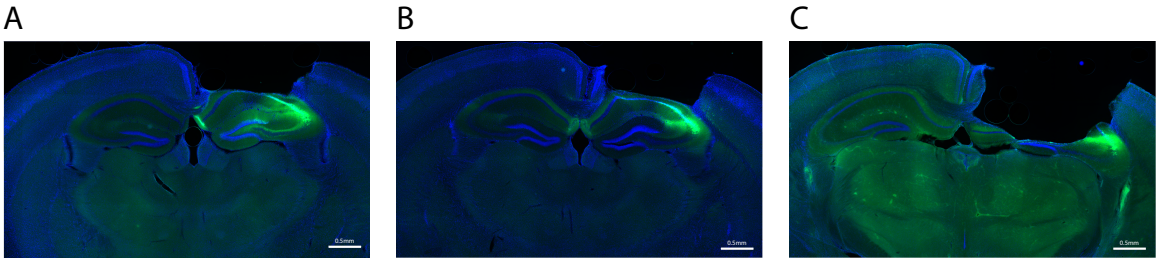

Figure 13. Histological analysis of GRIN lens implant. (A) Example of hippocampal section from animal showing CA1 GFP expression with good focus. (B) Example of hippocampal section from animal showing GFP expression in CA2 with poor focus. (C) Example of hippocampal section from animal showing no GFP expression due to lack of hippocampal cortex.

We then imaged brain slices taken from animals implanted with both the AAV and the GRIN lens. Four out of six animals implanted with the GRIN lens did not show precise expression of GFP in the CA1 region of the hippocampus during live imaging of animals anesthetized under 2% isoflurane solution. Histological analysis of brain slices taken from these animals shows that slices continue to express GFP but that expression sometimes ended up in the CA2 region of the hippocampus, thereby resulting in poor GRIN lens focusing during live imaging (Figure 13B). Furthermore, some tissues showed evidence of complete degeneration of hippocampal CA1 (Figure 13C). It is possible that the CA1 region of the cortex was aspirated during the GRIN lens implantation surgery, thus contributing to lack of GFP expression.

CHAPTER 3: DISCUSSION

Our results suggest that hippocampal CA1 and CA3 place cell physiology is impaired in CA3-APP models of AD. This was first seen with respect to behavioral impairments. Our CA3-APP animals all showed impaired ability to decide which direction to go during the spatial memory task in some capacity, where young and aged animals showed impairments during both the 2 and 10 second delay portions of the task (with worse impairments and ability to improve spatial memory being shown in aged animals) (Figure 5). This is consistent with the idea that AD is a progressive neurodegenerative disease that gets worse with age. Furthermore, our results corroborate previously existing data showing that AD animals have significant deficits in memory retrieval during memory tasks, where animals were shown to have worse behavioral deficits during the first trial of a new day rather than during the last trial of the previous day (Billings et al., 2005; Roy et al., 2016). After understanding that our genetic manipulations in hippocampal CA3 indeed caused impairments in hippocampal-dependent spatial memory consistent with other models of pan-neuronal dysfunction (other AD models), we sought to understand the mechanisms underlying such physiological impairments during spatial memory tasks. This was where our figure 8 maze setup played a crucial role in obtaining our results. Previous studies conducted by other researchers have commonly used random foraging tests, T-maze memory tasks, or the Morris water maze (Billings et al., 2005; Gimenez-Llort et al., 2007; Sterniczuk et al., 2010; Cacucci et al., 2008; Ciupek et al., 2015; Roy et al., 2016; Mably et al., 2016; Galloway et al., 2018). These tests did not directly allow for the analysis of place cell dysfunction while actually completing goal-oriented tasks either because of need for

experimenter intervention during the task (eg. being picked up off the maze between laps during the T maze, or the Morris water maze, where performing electrophysiology experiments in water can prove very difficult), or because the task itself only evaluated spatial properties by place cells, but did not look at spatial properties during goal-oriented tasks, such as with the random foraging tasks. That being said, novel techniques are being developed to better evaluate place cell properties of hippocampal dependent spatial navigation without perturbing the animal during the task, such as with the honeycomb maze (Wood et al., 2018). Our Figure 8 maze was effective at essentially creating a continuous version of the T-shaped memory task by allowing mice to run back to the central starting arm by themselves without being perturbed by experiments. This allowed us to record electrophysiology from cells during the task while remaining confident that the experimenter did not interfere with the experiments.

After establishing the reliability of our Figure 8 spatial memory task, we sought to understand how place cells in both the CA1 and CA3 regions of the hippocampus were affected by AD. We found that place cells in both cell layers are impaired across both young and aged animals expressing CA3-APP, particularly when tasks become more hippocampal dependent (shown by data gathered during the delay 10 periods on the figure 8 spatial memory task). Both young and aged CA3-APP animals showed significantly lower mean firing rates of CA1 cells, where aged CA3-APP animals also displayed lower mean firing rate distributions during the delay 10 portion of the task (Figures 6, 7). In the CA3 layer, CA3-APP animals generally showed significantly higher mean firing rates. CA3 place cell peak firing rate was generally greater in young CA3-APP animals and lower in aged CA3-APP animals during the ten second delay portion of

the task (Figures 6,7). Aged CA3-APP animals also showed lower information scores and higher across sides correlations for both CA1 and CA3 place cells during the ten second delay portion of the task (Figures 8, 9). Young CA3-APP animals paradoxically showed a lower across sides correlation in CA3 cells of young animals (though still higher across sides correlations in CA1 cells) (Figure 9). This was contrary to what we expected and could be as a result of a low sample size for CA3 cells (where there were much lower numbers of cells recorded in the CA3 region of young control animals). Further experiments looking at CA3 cells will need to analyze significantly greater numbers of cells in order to make more definitive conclusions about CA3 impairments during hippocampal tasks. CA1 and CA3 place cell stability across trials was also significantly impaired in aged CA3-APP animals during the ten second delay of the task (Figure 10). Finally, place fields in both young and aged CA3-APP animals were significantly higher in all CA3-APP animals, with the largest difference being shown in CA3 cells of aged CA3-APP animals (Figure 11).

Analysis of these metrics points towards significantly impaired precision of place cells while CA3-APP animals completed hippocampal-dependent goal-directed working memory tasks. Our results are consistent with the findings of previous research studies showing that hippocampal place cells during spatial memory tasks show impaired precision, particularly with respect to stability of place fields and information score, and synaptic plasticity (Cacucci et al., 2008; Cheng & Ji, 2013; Witton et al., 2014; Zhao et al., 2014; Ciupek et al., 2015; Booth et al., 2016). Our data builds upon this existing data by testing specific place cell impairments during goal-directed memory tasks without perturbing an animal (as would be the case in the water maze or the T-maze).

Furthermore, our results confirm findings showing CA1 place cells are significantly impaired during spatial coding, thus corroborating the results of Mably et al. (2016). Our experiments have added to these studies by analyzing both CA1 and CA3 place cells using tetrode wire electrophysiology while animals completed the figure 8 spatial memory task. Our results have conclusively shown impaired place cell activity in both the CA1 and CA3/DG regions of the hippocampus in CA3-APP mouse models. Earlier studies raised the question of which cell layer was more affected by AD-like pathology (Galloway et al., 2018). Galloway et al. found that the CA2 and CA3 regions of the hippocampus are more highly affected by AD progression than CA1 place cells, where their experiments did not find CA1 place cell impairments. Because most aforementioned studies use pan-neuronal models of AD, which express mutant Tau or APP everywhere in the brain, we cannot directly compare our results (which come from animals overexpressing APP only in hippocampal CA3) to studies like the ones performed by Galloway et al. and Mably et al. We can conclude, however, that CA3 neurons, which project to both CA3 itself and hippocampal CA1, are highly dysfunctional in CA3-APP mice. This effectively implies that projections within hippocampal CA3, which were impaired in our CA3-APP animals, could be very important to our spatial memory task. Coupled with our earlier results showing significant place cell impairment in hippocampal CA1, we have reason to believe that dysfunction in both cell layers is involved in early progression of AD. Our results can also be useful in elucidating differences in place cell impairment based on hippocampal cell layer and adds to a growing story of place cell dysfunction in AD pathology. Regardless, the difference in CA1 and CA3 place cell dysfunction in AD warrants further research into why

distinctions in impairments might exist, and how such impairments may affect progression of spatial memory loss in AD.

Our findings also add to a growing body of data analyzing SWR and theta modulation impairments of CA1 and CA3 neurons in AD models. Previous experiments reported abnormal theta modulation and SWR activity in mouse models of AD (Villette et al., 2010; Cantero et al., 2011; Scott et al., 2012; Cheng & Ji, 2013; Schneider et al., 2014; Cayzac et al., 2015; Ciupek et al., 2015; Booth et al., 2016; Gillepsie et al., 2016). Our experiments showing place cell dysfunction through decreased stability, decreased information score, increased place field size, and other spatial information metrics, show that place cell function is impaired in terms of not only theta and SWR rhythm, but also firing rate and coded information. Many of these previous studies analyzed how memory recall is affected in mouse models of AD, finding that impaired SWR rhythm and theta modulation may be to blame for impaired memory recall (Villette et al., 2014; Ciupek et al., 2015; Cayzac et al., 2015; Schneider et al., 2016; Booth et al., 2016; Mably et al., 2017). It thus follows that it could be useful to test SWR dysfunction in our CA3-APP animals during our figure 8 spatial memory task to elucidate how SWR impairments manifest themselves while animals perform goal-oriented memory tasks. Another variable that might be contributing to the deficits in behavior observed is the fact that place cells might not be reactivated during sleep, in particular during SWR, in the CA3-APP mice. Indeed, future research in our lab will analyze LFP and SWR data from CA1, CA3, and DG regions of the hippocampus during sleep before and after the memory task, as well as during the memory task in the hopes of being able to elucidate how SWR and

theta modulation abnormalities may play a role in memory loss progression in AD models.

Finally, we attempted to perform calcium imaging experiments on our AD mouse models to yield a more global view of hippocampal place cell dysfunction. Our initial injections of the GCaMP7f GECI showed promising results since histological analysis of most animals confirmed expression of the GFP fluorophore (Figure 12). However, when we attempted to image the animals *in vivo*, we were unable to confirm expression of GFP from several of our animals. We currently hypothesize that issues with the AAV injection and GRIN lens implantation surgery are to blame for the issue. Histological analysis of animals implanted with the GRIN lens showed significant degeneration of hippocampal tissue (which seems to be the cause of the lack of expression) (Figure 13C). It is possible that the GRIN lens implant surgery, which involved aspirating layers of cortex above the hippocampus may be to blame for this apparent lack of hippocampal cortex. Further investigation of the GRIN lens surgery will need to take place in order to perfect the implant and allow for *in vivo* recording of neuronal activity. Other possible reasons for lack of strong GFP CA1 imaging include imprecise injection of the AAV-GCaMP7f virus into the CA2 region of the hippocampus rather than the CA1 region (resulting in poor focus rather than lack of expression) (Figure 13B). We hypothesize that once corrections to both the AAV injection surgery, and the GRIN lens implantation surgery are achieved, we will be able to analyze sequences of neural firing, as well as look at how interactions between neurons may be impaired in models of AD. Indeed, such information would well complement existing tetrode wire electrophysiology data, which is unable to acquire information from many cells at once and cannot analyze sequences of neuronal firing.

Our results as a whole, combined with previously acquired data from mouse models of AD, point towards significantly impaired CA1 and CA3 place cell activity in mouse models of AD as they perform hippocampal dependent memory tasks. These data contribute to our understanding of memory loss progression in AD and, if combined with novel calcium imaging data, could pave the way towards understanding aberrant neural rhythms and activity in AD. The goal of this understanding would be to eventually develop novel therapeutic strategies targeted towards hippocampal dysfunction to restore healthy neural activity during early stages of AD.

CHAPTER 4: CONCLUSION

We found that both young and aged CA3-APP animals show significantly impaired performance during hippocampal dependent memory tasks. This was shown to be associated with impaired CA1 and CA3 place cell activity in the form of decreased information score, increased place field size, discrepancies in mean and peak firing rates, greater spatial correlation, and decreased place cell stability, particularly while the tasks became more hippocampal dependent. Our data suggests that such impairments are greater in aged mouse models, with particularly large differences being observed in the CA3 region of the hippocampus. Furthermore, our attempt at using calcium imaging to analyze large populations of CA1 neurons in CA3-APP animals was largely unsuccessful but paves the way for future research to utilize the technique to analyze neurons in the hippocampus. Our results indicate the place cell dysfunction may play a key role in memory loss progression in mouse models of AD, and add to previously existing data showing place cell dysfunction and SWR impairments in animal models of AD.

This thesis, in full, is currently being prepared for submission of publication of the material by Viana da Silva, Silvia; Haberl, Matthias G; Gaur, Kshitij S; Patel, Rina; Koo, Edward; Leutgeb, Jill K.; Leutgeb, Stefan. The author of this thesis will be a co-author of the publication.

REFERENCES

Ancolio, K., Dumanchin, S., Barelli, H., Warter, J.M., Brice, A., Campion, D., Frebourg, T., Checler, F. Unusual phenotypic alteration of beta amyloid precursor protein (betaAPP) maturation by new Val-t15→Met betaAPP-770 mutation responsible for probable early-onset Alzheimer's disease. *Proc. Natl Acad. Sci. USA* **96**(7), 4119-4124 (1999).

Buzsaki, G. *Rhythms of the Brain*. (Oxford University Press, 2006).

Billings, L.M, Oddo, S., Green, K.N., McGaugh, J.L., LaFerla, F.M. Intraneuronal Abeta causes the onset of early Alzheimer's disease related cognitive deficits in transgenic mice. *Neuron* **45**, 675–688 (2005).

Booth, C.A., Witton, J., Nowacki, J., Tsaneva-Atanasova, K., Jones, M.W., Randall, A.D., Brown, J.T. Altered intrinsic pyramidal neuron properties and pathway-specific synaptic dysfunction underlie aberrant hippocampal network function in a mouse model of tauopathy. *J. Neurosci* **36**, 350–363 (2016).

Cacucci, F., Yi M., Wills, T. J., Chapman, P. & O'Keefe, J. Place cell firing correlates with memory deficits and amyloid plaque burden in tg2576 alzheimer mouse model. *Proc. Natl. Acad. Sci.* **105**, 7863–7868 (2008).

Cai, D.J., Aharoni, D., Shuman, T., Shobe, J., Biane, J., Song, W., Wei, B., Veshkini, M., La-Vu, M., Lou, J., Flores, S.E., Kim, I., Sano, Y., Zhou, M., Baumgaertel, K., Lavi, A., Kamata, M., Tuszynski, M., Mayford, M., Peyman, G., Silva, A.J. A shared neural ensemble links distinct contextual memories encoded close in time. *Nature*, **534**(7605), 115–118 (2016).

Cai, X.D., Golde, T.E., Younkin, S.G. Reelase of excess amyloid beta protein from a mutant amyloid beta protein precursor. *Science* **259**(5094), 514-516 (1993).

Cantero, J.L., Moreno-Lopez, B., Portillo, F., Rubio, A., Hita-Yanez, E., Avila, J. Role of tau protein on neocortical and hippocampal oscillatory patterns. *Hippocampus* **21**, 827–834 (2011).

Cayzac, S., Mons, N., Ginguay, A., Allinquant, B., Jeantet, Y., Cho, Y.H. Altered hippocampal information coding and network synchrony in APP-PS1 mice. *Neurobiol. Aging* **36**, 3200–3213 (2015).

Chapman, P.F., White, G.L., Jones, M.W., Cooper-Blacketer, D., Marshall, V.J., Irizarry, M., Younkin, L., Good, M.A., Bliss, T.V., Hyman, B.T., Younkin, S.G., Hsiao, K.K. Impaired synaptic plasticity and learning in aged amyloid precursor protein transgenic mice. *Nat. Neurosci.* **2**, 271–276 (1999).

Chen, T.W., Wardill, T.J., Sun, Y., Pulver, S.R., Renninger, S.L., Baohan, A., Schreiter, E.R., Kerr, R.A., Orger, M.B., Jayaraman, V., Looger, L.L., Svoboda, K., Kim, D.S. Ultrasensitive fluorescent proteins for imaging neuronal activity. *Nature* **499,** 295–300 (2013).

Cheng, J. & Ji, D. Rigid firing sequences undermine spatial memory codes in a neurodegenerative mouse model. eLife 2:e00647 (2013).

Citron, M., Oltersdorf, T., Haass, C., McConlogue, L., Hung, A.Y., Seubert, P., Vigo-Pelfrey, C., Lieberburg, I., Selkoe, D.J. Mutation of beta-amyloid precursor protein in familial Alzheimer's disease increases beta-protein production. *Nature* **360**(6405), 672-674 (1992).

Citron, M., Vigo-Pelfrey, C., Teplow, D.B., Miller, C., Schenk, D., Johnston, J., Winblad, B., Venizelos, N., Lannfelt, L., Selkoe, D.J. Excessive production of amyloid-beta protein by peripheral cells of symptomatic and preymptomatic patients carrying the Swedish familial Alzheimer's disease mutation. *Proc. Natl Acad. Sci. USA* **91**(25), 11993-11997 (1994).

Ciupek, S.M., Cheng, J., Ali, Y.O., Lu, H.C., & Ji, D. Progressive functional impairments of hippocampal neurons in a tauopathy mouse model. *J. Neurosci.* **35**(21), 8118–8131 (2015).

De Strooper, B. & Annaert, W. Proteolytic processing and cell biological functions of the amyloid precursor protein. *J Cell Sci.* **113**, 1857–1870 (2000).

De Strooper, B., Simons, M., Multhaup, G., Van Leuven, F., Beyreuther, K., Dotti, C.G. Production of intracellular amyloid-containing fragments in hippocampal neurons expressing human amyloid precursor protein and protection against amyloidogenesis by subtle amino acid substitutions in the rodent sequence. *EMBO J.* **14**, 4932–4938 (1995).

Eichenbaum, H. Hippocampus: Cognitive Processes and Neural Representations that Underlie Declarative Memory. *Neuron* **44**, 109–120 (2004).

Fu, H., Rodriguez, G.A., Herman, M., Emrani, S., Nahmani, E., Barrett, G., Figueroa, H.Y., Goldberg, E., Hussaini, S.A., Duff, K.E. Tau Pathology Induces Excitatory Neuron Loss, Grid Cell Dysfunction, and Spatial Memory Deficits Reminiscent of Early Alzheimer's Disease. *Neuron* **93**(3), 533–541 (2017).

Furukawa, K., Barger, S.W., Blalock, E.M., Mattson, M.P. Activation of K+ channels and suppression of neuronal activity by secreted beta-amyloid-precursor protein. *Nature* **379**(6560), 74-8 (1996).

Fyhn, M., Molden, S., Witter, M.P., Moser E.I., Moser, M.B. Spatial representation in the entorhinal cortex. *Science* **305**, 1258-1264 (2004).

Galloway, C.R., Ravipati, K., Singh, S., Lebois, E.P., Cohen, R.M., Levey, A.I., Manns, J.R. Hippocampal place cell dysfunction and the effects of muscarinic m1 receptor agonism in a rat model of alzheimer's disease. *Hippocampus* (2018).

Ghosh, K.K., Burns, L.D., Cocker, E.D., Nimmerjahn, A., Ziv, Y., El Gamal, A., Schnitzer, M.J. Miniaturized integration of a fluorescence microscope. **Nat. Meth.** 8, 871–878 (2011).

Gillespie, A.K., Jones, E.A., Lin, Y.H., Karlsson, M.P., Kay, K., Yoon, S.Y., Tong, L.M., Nova, P., Carr, J.S., Frank, L.M., Huang, Y. Apolipoprotein E4 causes age-dependent disruption of slow gamma oscillations during hippocampal sharp-wave ripples. *Neuron* **90**, 740–751 (2016).

Gimenez-Llort, L., Blazquez, G., Canete, T., Johansson, B., Oddo, S., Tobena, A., LaFerla, F.M., Fernandez-Teruel, A. Modeling behavioral and neuronal symptoms of Alzheimer's disease in mice: A role for intraneuronal amyloid. *Neurosci. Biobehav. Rev.* **31**, 125–147 (2007).

Götz, J. & Ittner, L. M. (2008). Animal models of Alzheimer's disease and frontotemporal dementia. *Nat. Rev. Neurosci.* **9**, 532–544 (2008).

Grossi, D., Becker, J.T., Smith, C., Trojano, L. Memory for visuospatial patterns in Alzheimer's disease. *Psychol. Med.* **23**, 65-70 (1993).

Guariglia, C.C. Spatial working memory in Alzheimer's disease: A study using the Corsi block-tapping test. *Dementia & Neuropsychologia* **1**(4), 392-395 (2007).

Hardy, J.A., Higgins, G.A. Alzheimer's disease: the amyloid cascade hypothesis. *Science* **256**, 184–5 (1992).Johnston, J.A., Cowburn, R.F., Norgren, S., Wiehager, B., Venizelos, N., Winblad, B., Vigo-Pelfrey, C., Schenk, D., Lannfelt, L., O'Neill, C. Increased beta-amyloid release and levels of amyloid precursor protein (APP) in fibroblast cell lines from family members with the Swedish Alzheimer's disease APP670/671 mutation. *FEBS Lett.* **354**(3), 274-278 (1994).

Leutgeb, S., Leutgeb, J.K., Barnes, C.A., Moser, E.L., McNaughton, B.L., Moser, M.B. Independent Codes for Spatial and Episodic Memory in Hippocampal Neuronal Ensembles. *Science* **309**, 619–623 (2005).

Liu, L., Gauthier, L., Gauthier, S. Spatial disorientation in persons with early senile dementia of the Alzheimer's type. *Am. J. Occup. Ther.* **45**, 67-74 (1991).

Mably, A.J., Gereke, B.J., Jones, D.T. & Colgin, L.L. Impairments in spatial representations and rhythmic coordination of place cells in the 3xtg mouse model of alzheimer's disease. *Hippocampus* **27**, 378–392 (2017).

Mankin, E.A., Sparks, F.T., Slayyeh, B., Sutherland, R.J., Leutgeb, S., Leutgeb, J.K. Neuronal code for extended time in the hippocampus. *Proc. Natl Acad. Sci. USA* **109**, 19462-19467 (2012).

Matthews, K.A., Xu, W., Gaglioti, A.H., Holt, J.B., Croft, J.B., Mack, D., & McGuire, L.C. Racial and ethnic estimates of Alzheimer's disease and related dementias in the United States (2015–2060) in adults aged≥ 65 years. *Alzheimer's & Dementia* (2018).

Mattson, M.P., Cheng, B., Culwell, A.R., Esch, F.S., Lieberburg, I., Rydel, R.E. Evidence for excitoprotective and intraneuronal calcium-regulating roles for secreted forms of the beta-amyloid precursor protein. *Neuron* **10**(2), 243-54 (1993).

McNaughton, B.L. & Morris, R.G.M. Hippocampal synaptic enhancement and information storage within a distributed memory system. *Trends in Neurosciences* **10**, 408–415 (1987).

Miyawaki, A. & Tsien, R.Y. Monitoring protein conformations and interactions by fluorescence resonance energy transfer between mutants of green fluorescent protein. *Methods Enzymol.* **327**, 472–500 (2000).

Mu, Y. & Gage, F. Adult hippocampal neurogenesis and its role in Alzheimer's disease. *Mol. Neurodegener.* 6, 85 (2011).

Mullan, M., Crawford, F., Axelman, K., Houlden, H., Lilius, L., Winblad, B., Lannfelt, L. A pathogenic mutation for probable Alzheimer's disease in the APP gene at the N-terminus of beta-amyloid. *Nat. Genet.* **1**, 345–347 (1992).

Murrell, J., Farlow, M., Ghetti, B., Benson, M.D. A mutation in the amyloid precursor protein associated with hereditary Alzheimer's disease. *Science* **254**, 97–99 (1991).

Nádasdy, Z., Hirase, H., Czurkó, A., Csicsvari, J. & Buzsáki, G. Replay and time compression of recurring spike sequences in the hippocampus. *J. Neurosci.* **19,** 9497–9507 (1999).

Nilsberth, C., Westlind-Danielsson, A., Eckman, C.B., Condron, M.M., Axelman, K., Forsell, C., Stenh, C., Luthman, J., Teplow, D.B., Younkin, S.G., Naslund, J., Lannfelt, L. The 'Arctic' APP mutation (E693G) causes Alzheimer's disease by enhanced Abeta protofibril formation. *Nat. Neurosci.* **4**(9), 887-893 (2001).

O'Keefe, J. Place units in the hippocampus of the freely moving rat. *Experimental Neurology* **51**, 78–109 (1976) .

O'Keefe, J. & Dostrovsky, J. The hippocampus as a spatial map. Preliminary evidence from unit activity in the freely-moving rat. *Brain Res* **34**, 171-175 (1971).

O'Keefe, J. & Nadel, L. *The Hippocampus as a Cognitive Map*. (Oxford: Clarendon Press, 1978).

Pavlides, C. & Winson, J. Influences of hippocampal place cell firing in the awake state on the activity of these cells during subsequent sleep episodes. *J. Neurosci.* **9,** 2907–2918 (1989).

Ramon y Cajal, S. Histologie du systeme nerveux de l'homme et des vertebres. Paris: A. Maloine (1911).

Russell, J. T. Imaging calcium signals in vivo: a powerful tool in physiology and pharmacology. *Br J Pharmacol* **163,** 1605–1625 (2011).

Roher, A.E., Lowensen, J.D., Clarke, S., Woods, A.S., Cotter, R.J., Gowing, E., Ball, M.J. B-amyloid(1-42) is a major component of cerebrovascular amyloid deposits: implications for the pathology of Alzheimer's disease. *Proc. Natl Acad. Sci. USA* **90**, 10836-10840 (1993).

Roy, D.S, Arons, A., Mitchell, T.I., Pignatelli, M., Ryan, T.J., Tonegawa, S. Memory retrieval by activating engram cells in mouse models of early Alzheimer's disease. *Nature* **531**, 508–512 (2016).

Sabariego, M., Schonwald, A., Boublil, B.L., Zimmerman, D.T., Ahmadi, S., Gonzalez, N., Leibold, C., Clark, R.E., Leutgeb, J.K., Leutgeb, S. Time cells in hippocampus are neither dependent on medial entorhinal cortex inputs nor necessary for spatial working memory. *Neuron* doi: 10.1016/j.neuron.2019.04.005. (2019).

Schneider, F., Baldauf, K., Wetzel, W., Reymann, K.G. Behavioral and EEG changes in male 5xFAD mice. *Physiol. Behav.* **135**, 25–33 (2014).

Scheuner, D., Eckman, C., Jensen, M., Song, X., Citron, M., Suzuki, N., Bird, T.D., Hardy, J., Hutton, M., Kukull, W., Larson, E., Levy-Lahad, E., Viitanen, M., Peskind, E., Poorkaj, P., Schellenberg, G., Tanzi, R., Wasco, W., Lannfelt, L., Selkoe, D., Younkin, S. Secreted amyloid beta-protein similar to that of senile plaques of Alzheimer's disease is increased in vivo by the presenilin 1 and 2 and

APP mutations linked to familial Alzheimer's disease. *Nat Med.***2**(8), 864-870 (1996).

Scott, L., Feng, J., Kiss, T., Needle, E., Atchison, K., Kawabe, T.T., Milici, A.J., Hajos-Korcsok, E., Riddell, D., Hajos, M. Age-dependent disruption in hippocampal theta oscillation in amyloid-beta overproducing transgenic mice. *Neurobiol. Aging* **33**, 1481 e13–1481 e23 (2012).

Scoville, W. B. & Milner, B. LOSS OF RECENT MEMORY AFTER BILATERAL HIPPOCAMPAL LESIONS. *J Neurol Neurosurg Psychiatry* **20**, 11–21 (1957).

Selkoe, D.J. Alzheimer's disease: genes, proteins, and therapy. *Physiol. Rev.* **81**, 741-746

Skaggs, W. E. & McNaughton, B. L. Replay of Neuronal Firing Sequences in Rat Hippocampus During Sleep Following Spatial Experience. *Science* **271,** 1870–1873 (1996).

Sterniczuk, R., Antle, M.C., Laferla, F.M., Dyck, R.H. Characterization of the 3xTg-AD mouse model of Alzheimer's disease: Part 2. Behavioral and cognitive changes. *Brain Res.* **1348**, 149–155 (2010).

Tsien, J. Z., Chen, D.F., Gerber, D., Tom, C., Mercer, E.H., Anderson, D.J., Mayford, M., Kandel, E.R., Tonegawa, S. Subregion- and Cell Type–Restricted Gene Knockout in Mouse Brain. *Cell* **87,** 1317–1326 (1996).

Villette, V., Poindessous-Jazat, F., Simon, A., Lena, C., Roullot, E., Bellessort, B., Epelbaum, J., Dutar, P., Stephan, A. Decreased rhythmic GABAergic septal activity and memory-associated theta oscillations after hippocampal amyloid-beta pathology in the rat. *J Neurosci.* **30**, 10991–11003 (2010).

Weber, F. & Dan, Y. Circuit-based interrogation of sleep control. *Nature* **538,** 51–59 (2016).

Witton, J., Staniaszek, L.E., Bartsch, U., Randall, A.D., Jones, M.W., Brown, J.T. Disrupted hippocampal sharp-wave ripple-associated spike dynamics in a transgenic mouse model of dementia. *J. Physiol.* **594**(16), 4615–4630 (2015).

Wood, R. A., Bauza, M., Krupic, J., Burton, S., Delekate, A., Chan, D., & O'Keefe, J. (2018). The honeycomb maze provides a novel test to study hippocampal-dependent spatial navigation. *Nature* **554**(7690), 102–105 (2018).

Xu, C., Krabbe, S., Gründemann, J., Botta, P., Fadok, J.P., Osakada, F., Saur, D., Grewe, B.F., Schnitzer, M.J., Callaway, E.M., Lüthi, A. Distinct Hippocampal Pathways

Mediate Dissociable Roles of Context in Memory Retrieval. *Cell* **167,** 961–972 (2016).

Zhao, R., Fowler, S.W., Chiang, A.C., Ji, D., Jankowsky, J.L. Impairments in experience-dependent scaling and stability of hippocampal place fields limit spatial learning in a mouse model of Alzheimer's disease. *Hippocampus* **24**, 963–978 (2014).